The influence of the numerical approach on pre-augering on sheet pile design

Bachelor of Science Civil Engineering

N.J. van Dongen
n.j.vandongen@student.utwente.nl
S2545705

UNIVERSITY OF TWENTE.

10 July 2023

Preface

I am pleased to present to you my bachelor thesis, “The influence of the numerical approach on pre-augering on sheet pile design” as a graduation thesis to complete my academic journey in the Bachelor Civil Engineering at the University of Twente. This thesis is brought to you in cooperation between Fugro, the water department, and the University of Twente. I had some previous experience in dikes failure mechanisms during the bachelor classes, but it was nice to gain more knowledge from an industrial perspective instead of only the theoretical perspective. This thesis aims to combine the theoretical approach of analysing dike designs, and the applied characteristics of reinforcing dikes.

I would like to thank Milan Hinborch, my supervisor from Fugro, for assisting me in the process of getting to know the numerical analysis of reinforced designs and giving the necessary help obtaining the Fugro data hidden in the large network files. While also introducing me into the practical sides of civil engineering within a company. Moreover, I would like to thank Hongyang Cheng, my supervisor from University of Twente, for helping me through the difficult learning process of soil models, and the theoretical background of the complete analysis. And showing your enthusiasm for the soil mechanics.

I hope you enjoy reading this thesis and are informed by its statements.

Niels van Dongen

Executive summary

The effect of the installation technique pre-augering on the soil while installing sheet piles is a relatively unexplored area, while it has impacts on the final design of sheet piles. The current regulating standards consider a reduction factor that was based on the sheet pile installation technique of fluidization, while it is very likely the impact of these installation techniques on surrounding soils is very different. This study further analyses the difference between fluidization and pre-augering, and ultimately creates a quantitative analysis of this reduction area to increase the information available on pre-augering.

This research aims to analyze the impact of the method of numerically analyzing the dike sheet pile design on the final sheet pile length. But also analyzing the validity of the reduction factor assumption made by the POVM Publication longitudinal constructions (PPL). As the influence of this reduction factor can influence the sheet pile design and thus the safety of the residents living in proception of the dikes.

First, the validity of the reduction factor is reviewed, by observing the theory of both installation methods. Secondly, previously performed research is analysed to create a framework of experiments that should be performed. Then an accurate numerical model is made, using the base model of the Tiel-Waardenburg reinforcement project. Which is used to perform analysis on the effect of the method of implantation on the sheet pile length. The use of numerical analyses comes with several uncertainties including soil parameter variability, schematization of geometries, uncertainties within the soil model, etc. but generally shows reliable results. When implementing methods to take the inaccuracies into account.

After performing the numerical analysis, the reduction factor shows a significant trend with the sheet pile design. As the reduction factor decreases, the length of the sheet pile increase, whereas an increase in the reduction factor leads to a decrease in the length. This is primarily because the reduction factor directly influences the soil's stiffness and interface strength parameters, serving as a multiplier for these parameters. Consequently, a lower reduction value results in lower stiffness and interface strength parameters. While the reduction factor shows significant impacts on the sheet pile design, the area of the reduction factor, currently only considered inside the packed sand layer, is comparatively less significant. Nevertheless, some correlations are found resulting in some enlarging or reducing of sheet pile design.

The theory concerning fluidization and pre-augering, shows a very different effect occurring. The current assumption of the reduction factor is caused by a deficit in both fluidization and pre-augering knowledge. Nevertheless, the estimation of the pre-augering reduction factor should be further investigated, as the numerical analysis performed in this study shows the significant impact the reduction factor has on the sheet pile design, leading to shorter sheet piles, and creating a higher cost-effective sheet pile design.

Table of Contents

List of Figures

List of Tables

1. Introduction

In the field of geotechnical engineering, the design and construction of sheet pile walls are widely employed in various civil engineering applications to provide stability and support to structures. Sheet piles are efficient and cost-effective structural elements that find extensive use in the construction of retaining walls, deep excavations, waterfront structures, and even in dike reinforcement. The utilization of sheet piles in dike reinforcement has proven to be an effective approach to enhance the stability and resilience of these vital flood protection structures.

Sheet piles used in dike reinforcement act as structural elements that provide additional strength and stability to the embankments. They are installed along the water-facing side or within the core of the dike to enhance its overall resistance to water pressure and external loads. By driving the sheet piles into the ground, they create a continuous barrier that prevents water seepage and helps redistribute the forces acting on the dike.

The installation process of sheet piles for dike reinforcement is a crucial aspect of the construction procedure. It involves driving, vibrating, or pressing the sheet piles vertically into the ground to create a continuous barrier that enhances the dike's resistance to water pressure and external loads. However, in some unconventional cases, the ordinary methods do not suffice, for example, a site can contain restrictions in either space, regulations, or technical feasibility. In such instances, additional installation techniques are employed to overcome these challenges and ensure the successful reinforcement of dikes with sheet piles.

The utilization of additional methods such as fluidization and pre-augering in sheet pile installation has been found to loosen dense soils, as many leading piling companies suggest, such as Sheet Piling (UK) ltd., Fussey Piling, Ivor King and many more. This causes a decrease in the resistance encountered during the installation process. However, it is important to note that there is limited scientific research available on this particular topic, as highlighted by Nozaki (2018). Consequently, the precise effect of these additional methods on soil characteristics remains somewhat uncertain and requires further investigation. The variability of disturbed soil and the lack of comprehensive scientific studies contribute to the current knowledge gap in understanding the full implications of fluidization and pre-augering on soil behaviour during sheet pile installation.

As the leading expert on flood protection, the Netherlands has set regulatory measures concerning the fluidization and pre-augering method to ensure safety in all scenarios. The Hoogwater beschermingsprogramma (HWBP), translated to highwater protection program, is an alliance of the local water authorities and the Ministry of Infrastructure and Water Management. This partnership has initiated the development of the POVM Publication longitudinal constructions (PPL), a manual containing the knowledge of experts in dike reinforcement from many different organizations. The primary goal of the manual is to ensure safe dike reinforcement utilizing longitudinal constructions, like (anchored) sheet piles, bored pile walls, diaphragm walls, cofferdams, unreinforced soil mix-blocks, and anchor piles.

To return to the topic at hand, the PPL includes the disturbance of the soil induced by fluidization and pre-augering, as a reduction of soil stiffness of 50% during the analysis of the dike design using PLAXIS, a numerical finite element method (FEM) software. Nevertheless, as mentioned before, the knowledge available regarding the impact these additional methods have on soil characteristics remains limited. The reduction factor for both fluidization and pre-augering used in the PPL is based on one experimental research conducted in the Nederlek reinforcement program, where only

fluidization was used as a supplementary method (Arcadis, 2007). This raises the question of whether the same reduction factor of 0,50 can be used for both fluidization and pre-augering.

To further investigate the impact of pre-augering Fugro, has initiated an experiment during the Tiel-Waardenburg reinforcement program, where the effect of pre-augering on cone resistance is investigated. To assist Fugro in their conquest of understander the pre-augering behaviour, this paper aims to show how the method of numerically analyzing the reinforcement design can impact the design.

This paper first examines the theoretical differences between fluidization and pre-augering and evaluates the validity of the employment of a common reduction value in Chapter 2. Secondly, it will review the previous (corporate) research, due to la ack of scientific research, to explore the new knowledge acquired on this subject in Chapter 3. Chapter 4 shows the explanation of the numerical, which covers the soil models used, the soil properties, the different phases that were simulated, and the geometry used in the model. Chapter 5, explains the experiments that were performed using the base model. Chapter 6 discusses the results. And finally, Chapter 7 concludes the study.

2. Theory additional installation techniques

Fluidizing and pre-augering are two additional methods commonly used to support regular sheet pile installation methods in situations involving high-density or granular soils, where the conventional methods fall short. Although both methods serve similar purposes, which encompasses enhancing the efficiency and effectiveness of the installation process, they have distinct implementation methods, and the underlying physical processes are completely different. Despite these distinctions, the PPL suggests a common reduction factor for both methods. The PPL does include a difference in reduction factor area, the fluidization width is equal to the length of the sheet pile inserted into the sand layer, while the pre-augering width is equal to three times the auger diameter.

This chapter attempts to theoretically examine these methods, discern their dissimilarities, and evaluate the rationale behind the uniform reduction factor. Firstly, pre-augering is explained, then fluidization is discussed, and lastly, the dissimilarities will be addressed.

Pre-augering is an additional method to ensure the success of the implementation of the sheet pile reinforcement while pressing or vibrating the sheet pile into the ground. Pre-augering decreases the density of the soil, by augering into the soil and removing a minimal amount of soil. And thus create less resistance while pressing or vibrating the reinforcement into place. However, while pre-augering ensures execution success by loosening the soil (Lanting Wu, 2021), this consequently decreases the soil stiffness (Corrie Walton-Macaulay, 2018) to a certain degree which undeniably affects the behaviour of the reinforcement. In the worst-case scenario, the reinforcement will be insufficient in cases of extreme conditions.

2.1 Pre-augering

According to the Cambridge dictionary, drilling refers to the process of creating a hole in an object using a specialized tool. In pre-augering, which utilizes an auger as the specialized tool, this description is only partly accurate. While the use of an auger is often related to the creation of a hole, pre-augering deviates from this idea. Instead of physically removing soil and creating a hole, pre-augering involves a modified approach where the soil is not, or as little as possible, extracted.

An auger is used to facilitate the drilling in pre-augering, most companies use an auger diameter of 0.4m, but it ranges from 0.3 to 0.5m. Three different types of auger piles can be distinguished, depending on both the auger mechanics and the displacement behaviour. Full-displacement, partial-displacement, and non-displacement piles, however, to stay within the scope of this research non-displacement auger piles are covered more in-depth. In Figure 1 a schematic of the non-displacement auger is shown. By rotating the auger around its axis, the flight cuts into the soil while rotating, and it slowly moves into the ground without significant impact on the surrounding soil. Larisch (2012) describes screw auger action as a function between the cutting, transport and displacement of soil. The space between the auger flights is continuously filled with soil and using the principle from the Archimedean screw the soil slowly gets transported vertically towards the ground level. This transport depends on a multitude of factors, including the auger shape, geometry, and installation variables, like the rotation speed, and the torque. This allows the auger to move into the ground without disturbing the soil, while still removing the soil to create a hole.

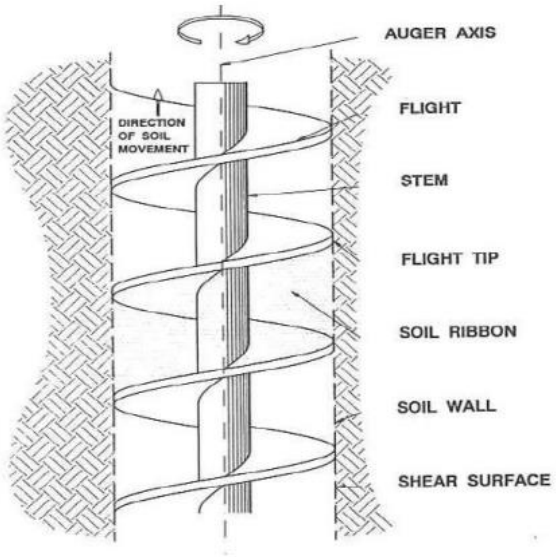

Figure 1: Basic schematic of a non-displacement auger after Thornburn, Greenwood and Fleming 1993 (Larisch, 2014)

The pre-augering uses these main functions described by Larisch partly. The displacement and transportation of the soil are not the goals in pre-augering, while these are considered the main functions of normal augering. With pre-augering, the goal is to reduce the compactness of the soil, without removing the soil in the drilled area. With the right conditions, the displacement and transport of soil can be reduced to a minimum, thus only cutting through the soil while forcing the auger into the ground. While cutting through the dense soil, the volume of the auger gets inserted into the compact soil together with a small amount of air, inducing dilation of the dense soil due to the movement of soil within the auger (S. Thorburn, 1993), thus, creating a soil with a higher void ratio, reducing the relative density. The soil resistance in loose sands is lower than in dense sands (Bingxiang Yuan, 2015). This aligns with the objective of pre-augering: to decrease resistance while pressing the sheet pile into position and mitigate installation issues. However, the amount of dilation, and to what extent this influences the resistance, remains unknown.

After the auger is inserted into the ground, the auger needs to be removed to initiate the sheet pile installation process. During the auger removal process, the main objective is to loosen the soil rather than actively remove it. To achieve this, the auger will be removed while rotating in the reserve direction, causing the soil to essentially fall off the auger flight and back into the drilled auger hole. As the soil retakes its place, it lacks the same level of compaction as before, preventing it from reforming into its previous dense soil structure (See Figure 3). Consequently, this process leads to a lower relative density of the soil compared to its initial state While the pre-augering method attempts to not extract any soil, to reduce the density within the soil a small amount of soil is removed to make place for the new void areas. In the pre-augering method, the goal is to minimize soil extraction. However, to achieve the desired reduction in soil density, a small amount of soil is deliberately removed to create space for the formation of new void areas.

Instead of using the auger in a continuous line along the sheet pile, when pre-augering is used in sheet pile installation only the interlocks between the sheet pile panels are pre-augered to create the loosened soil on the sheet pile's area with the most friction.

While theories provide a foundation for understanding construction practices, in the field of construction an emphasis on practical implantation is seen. Literature concerning the influenced zone around the auger remains limited. Thus, creating a gap in knowledge in the field, even though this

creates some uncertainties within the designs. While considering the theory explained above the following idealized schematic was found, shown in Figure 2. It should be noted that this schematic has no underlying research and is merely based on the theory explained above. The diameter of the influenced zone is unknown together with the actual reduction of soil strength. However, the figure indicates how the zone would shape.

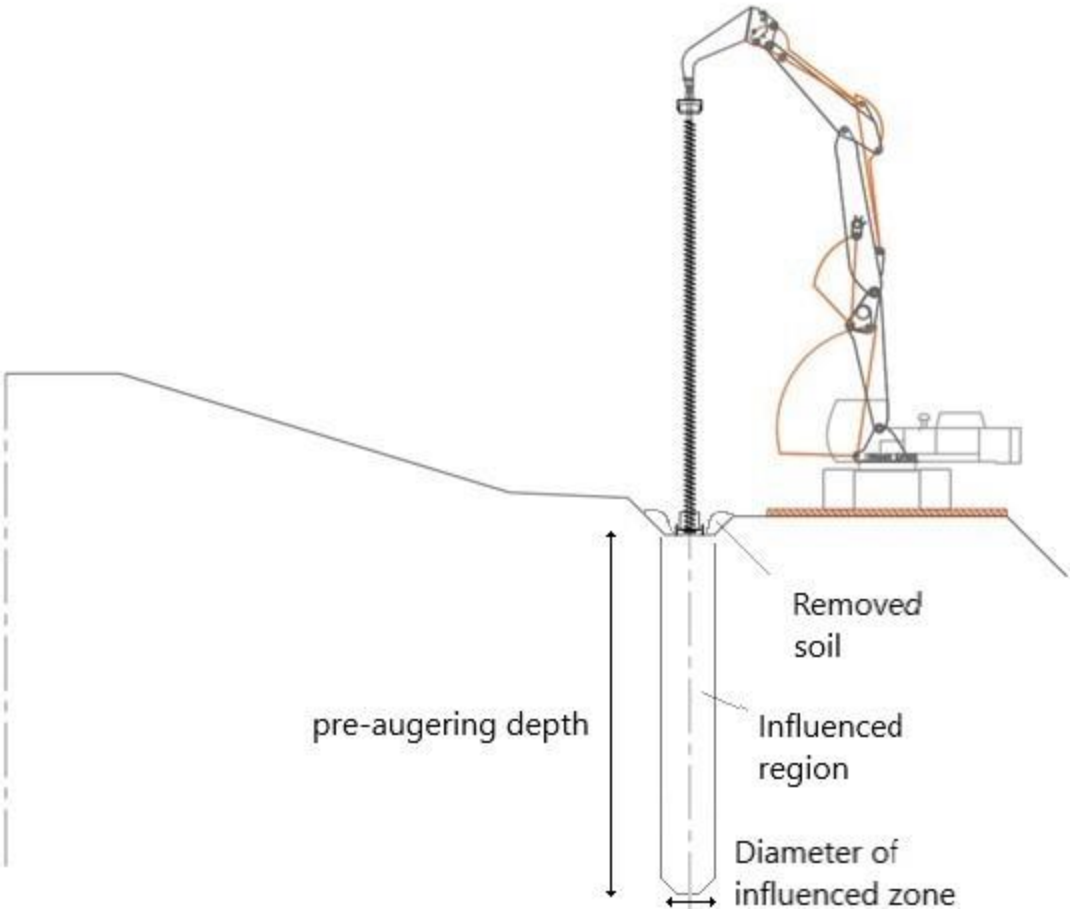

Figure 2: Schematized visualization of influenced area after augering

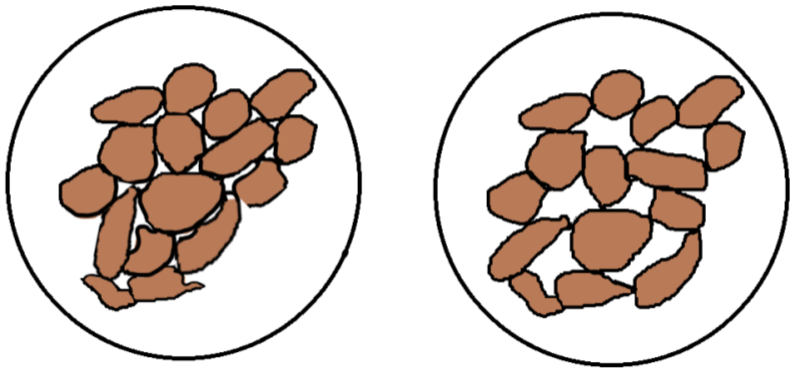

Figure 3: Schematized soil particles before and after pre-augering

2.2 Fluidization

Fluidization is similar to pre-augering an additional method of installation of sheet piles. It reduces the shaft friction of the soil surrounding the sheet pile, decreasing the necessary pressing force. However, the method of fluidization uses a completely different mechanic of soil.

Daizo Kunii (1991) describes fluidization as follows: “the operation by which solid particles are transformed into a fluidlike stat through suspension in a gas or liquid.”. The fluidization used in the installation of sheet piles uses water as a liquid to create the fluidized soil. When the fluid is passed through the soil at a low flow rate, the fluid only moves through the voids within the soil, while leaving particles stationary. Only when a higher flow rate is used, some particles will disperse in restricted regions due to the pressure caused by the fluid. At a larger increase in fluid velocity, all particles are suspended. Kunii explains this as the frictional force between particle and fluid counterbalances the weight of the particles, where the vertical component of the compressive force between adjacent particles disappears. This results in an incipiently fluidized bed, the vertical settlement of the soil particles no longer occurs, so moving through the soil can be done with relatively little force. The figure below displays the effects of increasing the flow rate on the state of the soil. Low velocity has barely any effect, while slowly increasing the flow rate causes the suspension and therefore increase in volume.

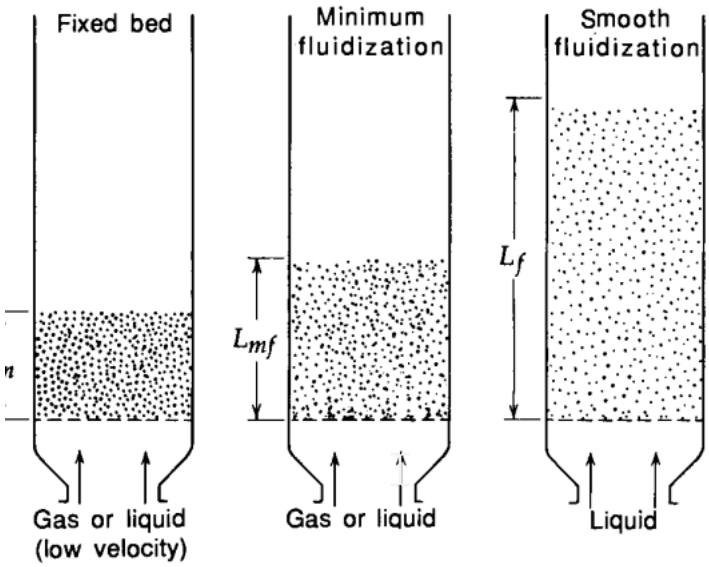

Figure 4: Various forms of contacting of a batch of solids by fluid ((Daizo Kunii, 1991)

In this method, a nozzle, connected to a tube and pump, is affixed to the toe of the sheet pile. As the pile is gradually lowered into place, the nozzle at the toe creates localized fluidized soil in the surrounding area by discharging water into the soil. This fluidization generates an overpressure, reducing the effective stress and facilitating the temporary fluidization of each layer in successive timesteps.

Further research has been done investigating the affected zone while using fluidizing in natural soils. Passini (2018) shows an overview of the mechanism of fluidization of sands in pile installation in saturated soils. And shows fluidization produces a large, disturbed region around the pile in the form of a jet hole. (Tsinker, 1988) suggested that the diameter of the fluidized zone can be as large as 20 times the diameter of the pile. Increasing with flow rate, jet velocity and the Froude number of particles. Passini and Schnaid (2015) further analysed the water jet fluidization mechanism in pile

installation, illustrated in Figure 5. The geometry of fluidized soil is in theory a relatively axisymmetric flow around the pile surrounded by nonfluidized soil.

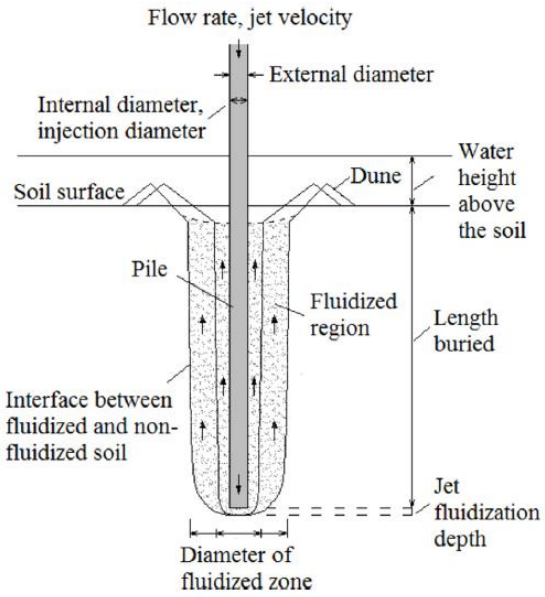

Figure 5: fluidization mechanism, and area of influence (Passini L B, 2015)

While the theory described by Kunii (1991) gives a base view of the fluidization process and Passini (2018) illustrated the water jet fluidization in saturated soils, the application of water jet fluidization in sheet pile installation within dikes is different. Arcadis (2007) mentions that, in the context of sheet pile installation, while using fluidization the movement of sand particles is not allowed. By controlling the discharge and pressure, the transportation of particles can be reduced to a minimum. Unlike the water jet as described in Passini, where soil transport along the pile occurs, this is not allowed in dike reinforcement due to the increased likelihood of other failure mechanisms. Nevertheless, it can be assumed that the shape of the fluidized region is like Passini displayed, as the fundamental process of fluidization remains similar However, it is arguable that the size and order of magnitude differ under unsaturated conditions and lower flow rates.

The application of fluidization in dike reinforcement projects only covers a small amount of the total dike reinforcement projects. So, the utilization of the method remains limited, and only little public research is available. The previously presented study shows a general indication of the theory behind water jet fluidization and displays an inherent difference between the additional installation methods. Further theorization of the application of fluidization in sheet pile installation is not pursued. As the general conceptualization given shows enough deviations.

2.3 Differences

Upon comparing both schematized representations of the fluidized region and the pre-augered region they exhibit similar shapes. However, both methods fundamentally differ from each other. Pre-augering involves tossing the soil around and consequently increasing the void ratio, while fluidization entails the internal insertion of water to disrupt the compactness and structure of the soil particles. Both methods achieve a state of reduced density by disrupting the soil structure and compactness. Nevertheless, assuming that both methods result in an equal reduction in density would be short-sighted. Many different factors come into play while disrupting the soil, which can result in very variable results, especially when using these different methods.

Unfortunately, due to limited information available on the general process of pre-augering and the specific case of fluidization in above-ground conditions, it is challenging to determine the size of the region. Additionally, the magnitude of the soil reduction in stiffness can only be estimated, as precise information is lacking. This lack of information shows the reasoning behind the current reduction factor of pre-augering in the PPL, the little knowledge of the effect of pre-augering forced the writers to estimate it. Considering this, taking the fluidization factor is a logical option as the result of the method remains similar.

The PPL however did make a distinction between areas of reduction size. This difference in size aligns with the theoretical understanding described earlier. While the fluidized area could be taken from the experimental research by Arcadis (2007), it would be unwise to use the same area based on the theory of pre-augering. the expected impact area of pre-augering would primarily involve the borehole and potentially the immediate surrounding regions due to minimal soil wall collapse. To ensure sufficient precaution, it is recommended in the PPL to implement a reduction factor area that is three times the diameter of the auger. Based on the contents of this chapter the PPL has used accurate estimation based on the information available, however, it would be advisable to further investigate both methods in the case of dike reinforcement programs. To create a better reduction value based on research instead of approaching estimates.

3 Literature research

The installation methods employed for sheet piles, such as fluidizing and pre-augering, are intriguing yet understudied. Although these techniques are sometimes essential to apply, the effects are quite unknown. The impact of pre-augering specifically in dike reinforcement programs is entirely unknown in international research publications. However, Dutch water authorities are keenly interested in the possibility to apply the techniques safely, while private companies prioritize cost-effectiveness. When the effect of pre-augering can be safely reduced, the reinforcement costs will reduce. So, both the water authorities and companies, albeit for different reasons, share an interest in understanding the effect. Consequently, both parties have conducted some research to quantify the effect on the soil's stiffness.

The experiments described below follow similar experimental setups. Firstly, the cone resistance of the soils in the dike is determined using a CPT. Then when the baseline is found, the installation process can begin, where the sheet piles are pressed or vibrated into the dike's soil. To see the effect of the installation method, more CPTs are used to find the cone resistance post-installation.

3.1 Nederlek

This research focussed on the effect of fluidization on the soil's cone resistance after the installation had taken place. The test used two different test locations, one on 3.25m from the sheet pile, and one next to the sheet pile. The research suggests that the cone resistance decreased by around 50%-60% from the top of the sand layer to the toe of the sheet pile. In the area beneath the toe of the sheet pile, the only influence detected was next to the sheet pile, while in the CPT at a 3.25m distance, this reduction did not occur, see Figure 6. Due to the low number of probes, an accurate representation of the "bubble" cannot be formed. Frustratingly, the report does not mention the exact depth of the influenced zone below the sheet pile. The total area of reduced cone resistance due to fluidization is assumed to reach further than the 3,25 m measured, an estimate of 5m is given. But again, due to the limited amount of CPTs, the estimation has not been verified.

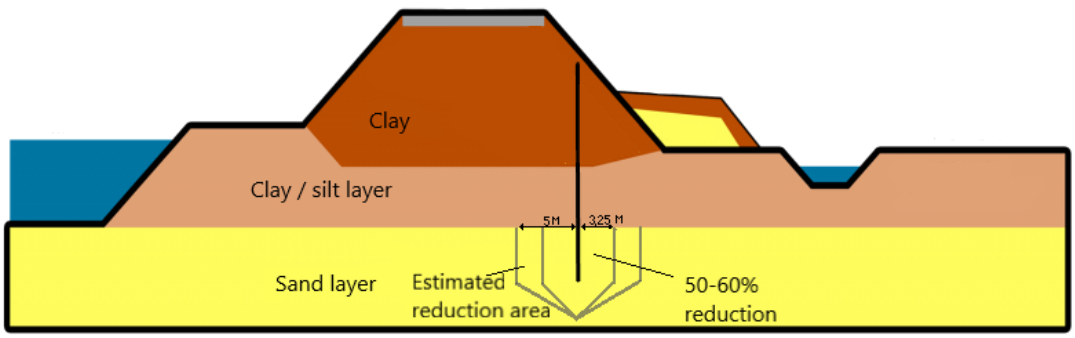

Figure 6: schematized area of reduction described by Arcadis (2007)

3.2 Vianen-Hazelaarplein

While the previous research was the base of the currently standing factor, the following experiment has been performed to gain more knowledge into the effect of fluidizing. Waterschap Rivierenland has tested the effect of fluidizing on the cone resistance during the Vianen Hazelaarplein reinforcements. This experiment was expanded as 9 CPT locations were used to further analyse the effect in more detail. A CPT was taken at 0.5, 1.0 and 2.0 m from the sheet pile, on three separate locations with circa 2.0 m between every row.

Whereas Arcadis (2007) suggested the reduction of cone resistance due to fluidization is around 50-60% in a 5m range. Kames (2021) found that from the top of the sand layer to the toe of the sheet pile the reduction changes depended on the distance to the sheet pile. The 0.5m distance gives an average increase in cone resistance of +15%. The 1.0m distance gives a decrease of -7.87%. and the 2.0m distance gives a decrease of -15.03%. When considering the area below the sheet pile, other values were found. At 0.5m almost no reduction of cone resistance was found, only a 1% reduction. At 1.0 m a significant difference of -42.58% was found. And at 2,0m the reduction is close to 0% again with a reduction of 0.13%.

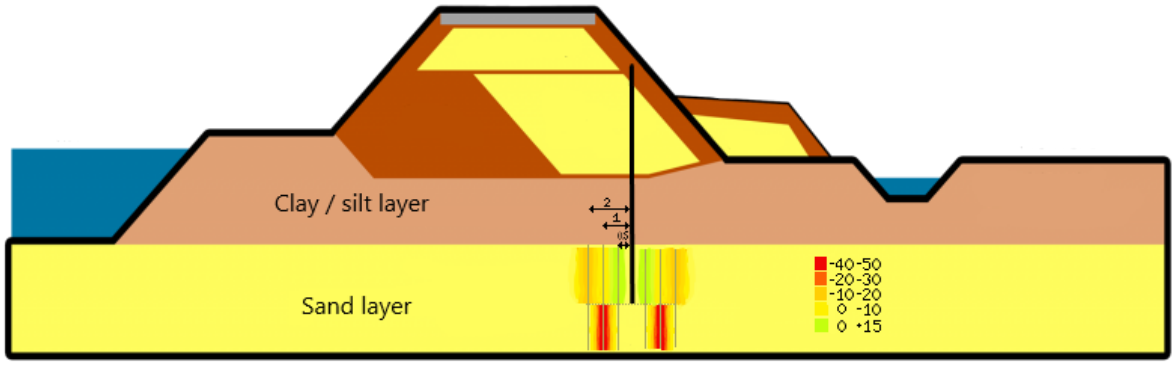

Figure 7: Effect of fluidizing on cone resistance according to Arcadis (2007)

The two different fluidization experiments give very different results. While Arcadis found that the cone resistance reduces around 50-60% over a range of at least 5m, Kames found that the largest reduction of 42% is located underneath the toe of the sheet pile at a distance of 1.0m, while the other locations experience no loss more than 20%, and even increases in some cases.

The two projects differ from each other in multiple parts, which could explain the different results. As well as the high variability in soils plays a large part. Kames (2021) has put the general characteristics of both projects side to side in Table 6. The most significant differences are, firstly the discharge of the fluidizing in the sand layer, where the Nederlek project used a mean discharge of 150l/min whereas the Vianen Hazelaar project used only 70l/min, a difference of more than 50%. Secondly, the mean Qc at the retainment was also around twice as much. Another major factor of variability is the use of vibratory hammers in combination with fluidization, both research studies used the combination. Previous research done by Linger (1963) shows the effect of vibration on volume change, which impacts the compactness and cone resistance of the soil. These differences can play a large part in the results.

3.3 Wolferen-Sprok

The most interesting study to examine the effect of pre-augering and therefore the reduction value is the Wolferen-Sprok reinforcement research. In this project, the effect of pre-augering on the cone resistance was investigated, and a similar protocol was used as for the fluidization experiments. First, a pre-CPT is done to create a base scenario at the sheet pile, then after the installation of the sheet pile, four post-CPTs are done. From 0-, 0.5-, 1.0-, and 2.0-meter distance from the sheet pile. This is done at two locations. It should be noted that in this experiment vibration was used as the installation method, which could influence the results. The auger used in this experiment had a diameter of 300mm. Using sheet piles of 12m, and CPTs of 15m giving results up to 3 meters below the toe of the sheet pile.

The results of the two experiment locations, named DKMP3 and DKMP4, are shown in the graphs below, where left the cone resistance and on the right the friction ratio is shown. The numbers indicate some interesting areas where change is visible, the same numbers are visible in the corresponding figures.

DKMP3

1. The area right below the top layer made of clay the reduction of cone resistance is immediately seen especially in the close range, so 0-, 0.5-meter distance. However, still, some effects can be seen at further distances.
2. In the top of the sand layer, but also between +3.0 and 0.0 NAP an increase in friction ratio is seen. This might indicate the pre-augering had transported some clay from the top layer to the sand layers. Especially since the increase in friction ratio only takes place at the sheet pile, and to a smaller degree at a 0.5-meter distance.
3. The post CPTs at 0 and 0.5m distance are very similar until 2.0 NAP, from this length onwards the cone resistances show different values. This might be because due to natural variability. Or show an already decreasing effect of pre-augering and vibration at a small distance of 0.5m
4. At 3.0 to 0.0 NAP there does not seem to be a large difference between the cone resistance from before the installation of sheet piles and after at a 1.0- and 2.0-meter distance. Meaning the effect of pre-augering and vibration only reaches 1.0 meters from the sheet pile in some layers of soil.
   It also can be seen that the cone resistance increases at 0.5 and 1.0 meters from the sheet pile. This could be due to the vibration just like Linger (1963) has shown.

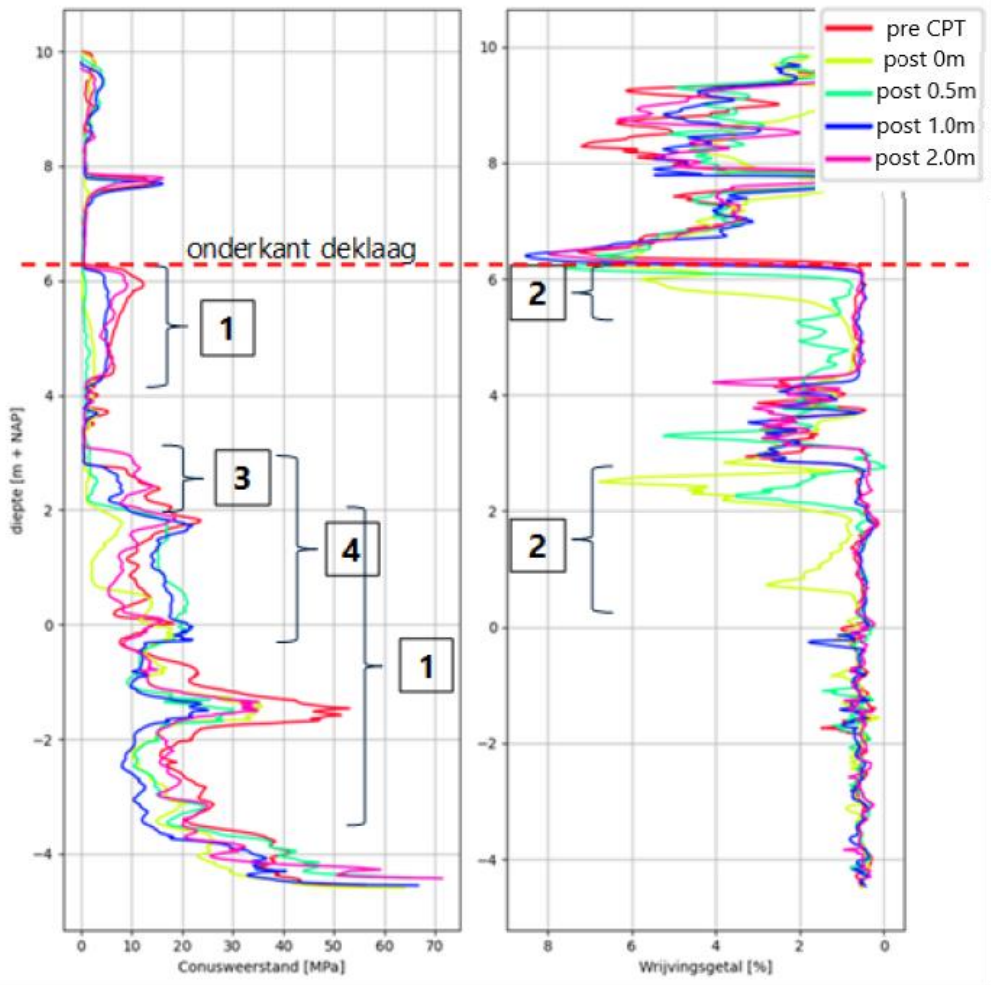

Figure 8: DKMP3 CPT results,
left cone resistance, right friction ratio

DKMP4

1. In the top layer an overall slight decrease in cone resistance is seen at every distance. This can be attributed to the pre-augering, as some soil from the top layer could be removed due to the auger.
2. At around 6.0 NAP first a decrease in cone resistance is visible, but around 5.0 NAP this decrease transforms into an increase. This could be caused by the auger moving clay from the top layer to the sand layer, which would increase the density of the soil, and therefore the cone resistance. This is also in line with the decrease in cone resistance at 1, where less clay is located after the installation
3. The effect that clay has been transported to the lower soil layers is seen at this location too, however, it is significantly less visible in comparison to DKMP3
4. The cone resistance has increased at around 2.0 NAP, which could be due to the vibrations while installing the sheet pile.
5. At -1.0 to -3.0 NAP a decrease of cone resistance can be seen, this could be an effect of the combination of pre-augering and vibration.

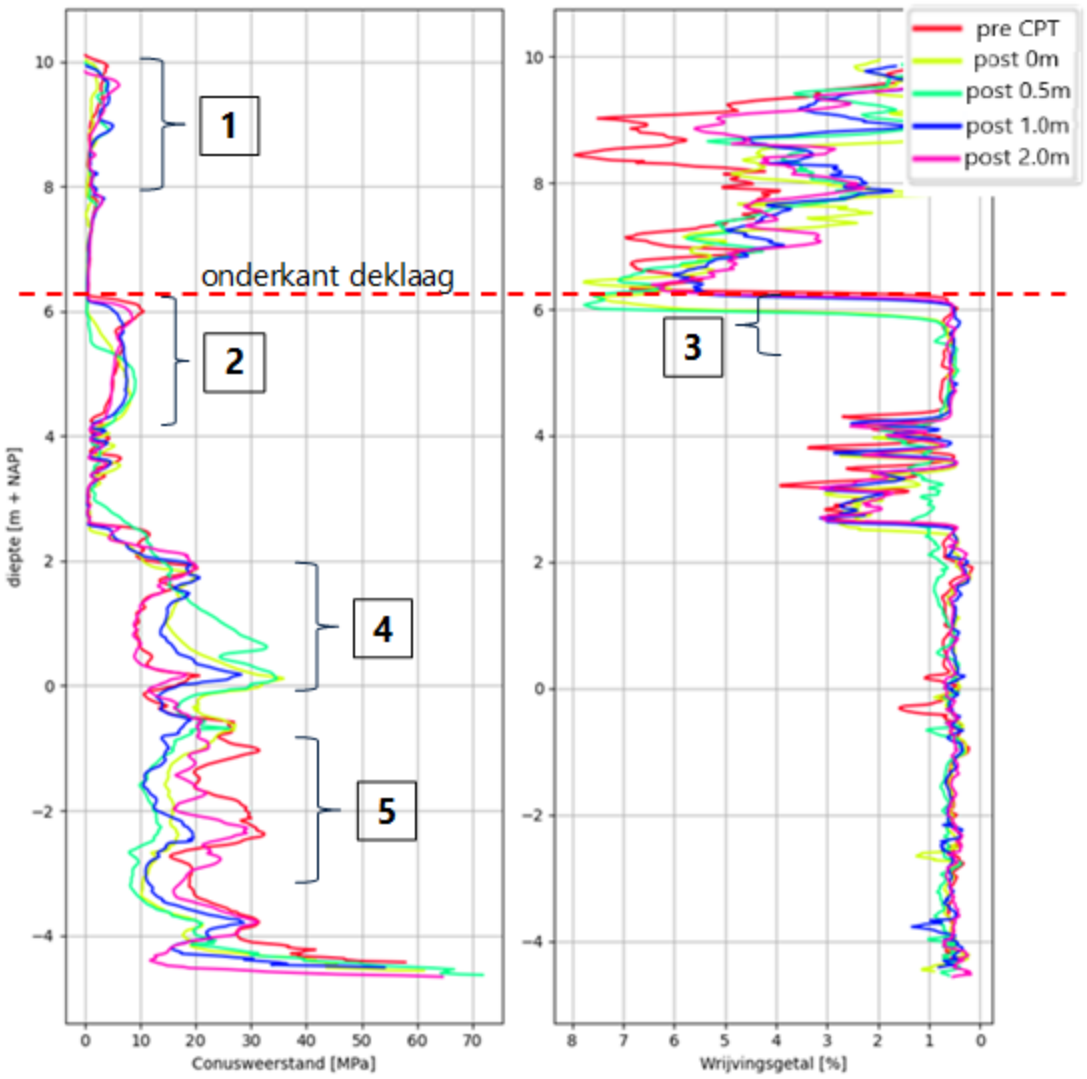

Figure 9: DKMP4 CPT results,
left cone resistance, right friction ratio

The overall results of this research contain a high amount of variability due to the combination of vibration and pre-augering giving a situation where it is unknown which installation method contributed to the change. Moreover, this specific case installed plastic sheet piles. To do this a supporting steel sheet pile was utilized, however, this steel had to be removed after the installation, which might additionally influence the data. Appendix A shows the mean cone resistance and the percentual difference at the location of the sheet pile, from before and after installation. In these tables, the difference in cone resistance ranges from a decrease of -80% to an increase of +47%. Also, the probes at 0.5-, 1.0, and 2.0-meter do not have a base measurement, so the natural variability of soil has not been addressed, however, at such close distances, it could be argued that the effect is negligible.

DKMP3 shows a mean percentual change of -39,9% over the sand layer, while DKMP4 shows a difference of +11,56% essentially making the soil stronger.

3.4 Discussion

These studies show high variability in the effect of cone resistance. But these form the basis for the decisions on which reduction values should be investigated. Firstly, the fluidizing studies were incorporated to see the origin of the reduction factor, however, due to the inherent differences between pre-augering and fluidizing the main ideas were taken from the Wolferen-Sprok study as it is the only study covering pre-augering.

The current standards suggest a reduction factor of 0.5, on a square area with the depth of pre-augering, and a width of three times the auger diameter. While the current regulation only incorporates the distance of pre-augering until the toe of the sheet pile, the literature suggests an affected area underneath the sheet pile up to at least 3m. The impact of this oversight will be analysed by including a reduction factor area underneath the sheet pile toe.

The width of the reduction factor area currently is three times the auger's diameter. This is backed by the literature, as on 1.0m from the sheet pile differences are seen, while from 2.0m no notable differences are observed. To analyse the impact of different auger sizes a variation in width will still be analysed.

Some soil parts are observed to increase in cone resistance while others decrease by 80%. However, the reduction of 80% is not representative of the entire sand layer, as only a small area has reduced like that, however, it does show the possibility of high reductions within the soil. Thus, the maximum reduction factor chosen to be analysed is 60%, resulting in a reduction factor of 0.40. On the other side, the biggest reduction factor is chosen based on the largest mean reduction over the complete sand layer, 40%, to ensure the safety of dikes the largest decrease was taken instead of the increase. Resulting in a reduction factor of 0.60.

4 Finite element method

To analyse the effect of the reduction factor due to pre-augering on the dike reinforcement the usage of finite element method (FEM) software PLAXIS 2022 is used. The software is widely used in the field of geotechnical engineering to analyse geotechnical problems ranging from excavation, foundations, embankments, and tunnels. The HWBP advises the usage of PLAXIS in the designing of reinforcements in dikes. PLAXIS has specialized features that are essential to the analysis of dikes. Dike reinforcement involves complex soil-structure interaction, especially in sheet pile reinforcement. But also requires a manner of modelling soil behaviour, groundwater flows, and stability analysis. PLAXIS offers robust numerical algorithms that can be used to accurately model dike behaviour during different life stages of the dike. It enables the simulation of consolidation, seepage, slope stability, and the interaction between sheet pile reinforcement and soil.

The model used in this analysis is based on the current reinforcement project TiWa which Fugro is working on. The main reason this model was chosen as a baseline is that this project contains the locations where the next pre-augering test will be performed by Fugro. Moreover, this is a situation where all geotechnical properties have been discovered in laboratories and creates a model based on a realistic situation where an initial design has been made.

The model will be explained in detail using the following subchapters. First discussing, the general geometry and soil layers. Secondly, the soil models and parameters used are shown and explained. Lastly, the different calculation steps to simulate all the life stages of the dike are discussed, where also the stability of the dike will be found.

4.1 Geometry model

The geometry of a dike model is of utmost importance due to its significant impact on the structural integrity and effectiveness of the dike system. As mentioned before the base of this model is based on the TiWa reinforcement program. The figure below illustrates the dike cross-section TG029 at Passewaaij, showcasing both the current layout and the recommended heightening. Throughout the dike's lifespan, the numerical model considers several different phases, changing the model's properties appropriately. However, this chapter will primarily focus on the initial model, including its soil layers, as the changes in geometry occur incrementally and are discussed in Section 4.5.

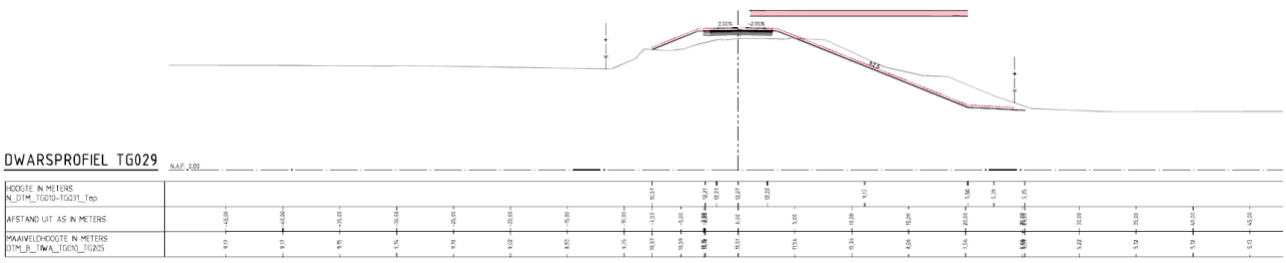

Figure 10: Cross section TG029 in compartment D of the TiWa reinforcement project

In addition to the basic cross-section, the dike model incorporates detailed soil layering. Figure 11 illustrates the soil layers at DWP190 TG029, which are then implemented in the combined initial PLAXIS model depicted in Figure 12. It is important to note a few details when viewing the initial model. Firstly, the colours used in the illustration differentiate different soil types, the same soil types seen in Figure 11 are utilized within the model. However, there are some modifications: for the middle Clay Silty 16-17,5kN/m3, the model is divided into three parts: the left side (frontal), the middle (crest),

and the right side (behind). Each section is assigned a different Pre-Overburden Pressures (POP), based on borehole tests performed while analysing the dike. The left side has a POP of $15kN/m^2$, the crest has a POP of $19kN/m^2$, and the right side a POP of $26kN/m^2$. Also, the left side of the dike has been filled with Clay Silty Sandy >17,5 kN/m3, instead of the dike material. Because dike material in practice only gets used inside the dikes.

Secondly, the grey-outlined elements in Figure 12, are elements that have not been activated, but are used in different calculation stages, explained in Section 4.5. These are the sheet pile, the anchor, the base spring, and the vehicle loads. As a base design, an AZ24-700 sheet pile with a length of 14.14m, in combination with a 12m HTAB 101/20 anchor was used. While they are visible in the initial stage, they are activated during the 2nd phase. The geometry for every different phase can be viewed in Appendix E, where also a detailed explanation of what happens during these stages is given.

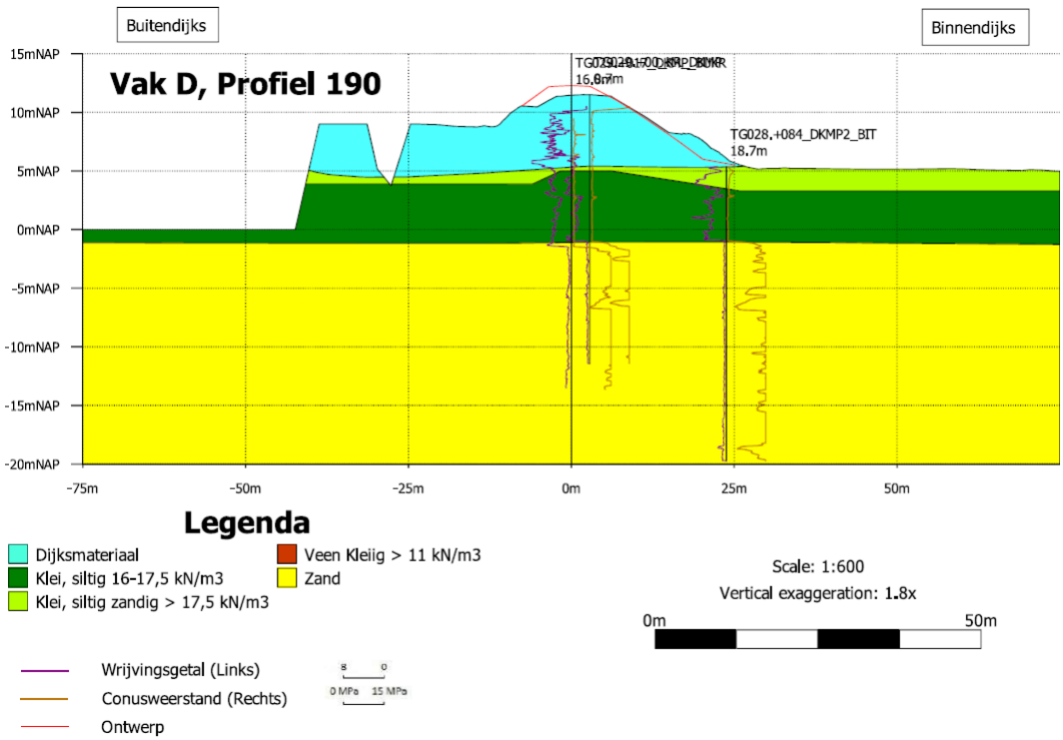

Figure 11: Cross-section DWP190 including soil layers

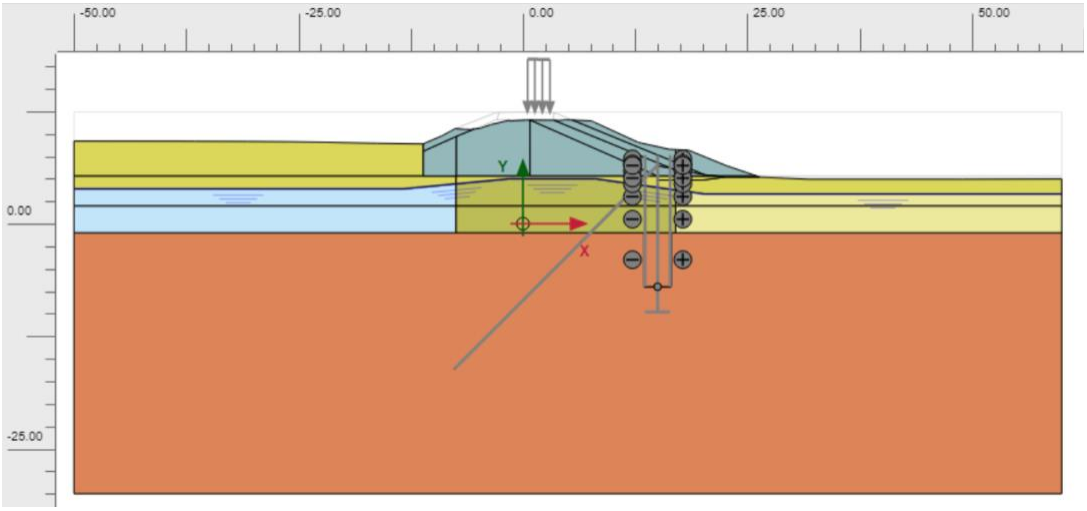

Figure 12: Initial state of the PLAXIS model

4.2 Soil models

During the analysis of the dike's reinforcement design, multiple soil models are used to describe the soil's behaviour under loads. For drained conditions, both the Hardening Soil (HS) model and the Soft Soil Creep (SSC) are used. Where the sand layers are modelled using the HS model is used, while for the softer soil like clay or sandy clay, the SSC model is used. When undrained conditions are applied the SSC model is converted to the SHANSEP NGI-ADP model.

The SSC model, first described by Vermeer & Neher (1999), is mostly used to incorporate the creep behaviour that soft soils show during a period without external loading. The SSC model has incorporated a time parameter to include the time-depend deformation of soil during an unloaded period, this ensures that the SSC model contains the features to include the settlement of the dike that is simulated in phase 1 where the current situation is modelled (see section 0). Moreover, additional advantages of the SSC are the better fit on triaxial and oedometer tests (PPL, 2020), and the inclusion of a variable 'cap', called 'cap hardening'. Which models the soil's behaviour that increases the variability in plastic deformation dependent on the stress history of the soil.

The HS model (Schanz T, 1999) is used to model the sand layers in the dike. Unlike clay sands do not show the creep behaviour so the SSC model is not applicable on the sand layers within the dike. The HS model includes a nonlinear stress-strain behaviour to a further extent than SSC. While the HS also has included cap hardening in the model, it also includes shear hardening. The shear hardening is modelled by varying the yield surface based on the deviatoric stresses.

The SHANSEP NGI-ADP model (Panagoulias S, 2018) is used to model the clays during undrained conditions. The NGI-ADP model is, in contrast to the previously mentioned models, a total stress model. This means the stress includes the pore water pressure, and therefore can directly calculate the undrained shear strength, whereas the HS or the SSC model can only obtain the undrained characteristics indirectly. The anisotropy of undrained shear strength and stiffness is incorporated within the model, and an exact match with the design undrained shear strength profiles is found. The original NGI-ADP model found by Grimstad et al. (2011) is slightly modified to feature the ability to simulate potential changes of the undrained shear strength based on the effective stress state.

These three soil models form the foundation of the FEM analysis. Each model is explained in more detail in Appendix B. Soil models. For the full implementation, one can view the PLAXIS material model manual (Bentley, 2020).

4.3 Structure models

For the reinforcement constructions simple elastic models have been applied to find the behaviour of the reinforcement. Due to a gap in knowledge on how to utilize the plastic capacity of steel sheet piles only elastic properties have been used (PPL, 2020). The anchor, the sheet pile, and the base spring have been modelled using pure elastic models, a detailed explanation is found in Appendix C.

4.4 Soil parameters

With the use of the soil models, the behaviour of the soil within the dike is given. However, the stand-alone models cannot be used to describe the behaviour of a particular soil interaction within the dike. The soil parameters describe the essential characteristics of the soil, as described in the previous chapter. The soil parameters used are gathered by Waterschap Rivierenland for the dike reinforcement projects along the Waal, therefore including project TiWa (Waterschap Rivierenland, 2020). Each model requires their own set of input parameters. Thus, the chapter is again split into subchapters covering each model.

The most notable parameters in this study are the HS stiffness parameter E_{50}^{ref}, E_{oed}^{ref}, and E_{ur}^{ref} and the strength parameter R_{inter}, which can be interpreted as the wall friction angle also used in the D-sheet piling software which is used since 1990 to complete sheet pile calculations (Deltares, 2023). These are the parameters influenced by the reduction factor caused by the pre-augering.

4.4.1 SSC

Table 1: Material properties Soft Soil Creep model

SOFT SOIL CREEP (SSC)	Weight		Strength parameters				Stiffness parameters			others	
Material	γ_{unsat} [kN/m³]	γ_{sat} [kN/m³]	c'_{ref} [kPa]	φ' [°]	ψ [°]	R_{inter} [-]	λ* [-]	κ* [-]	μ* [-]	ν'_{ur} [-]	K_0 [-]
Clay Silty 16-17,5 kN/m3	16,82	16,82	0	31,4	0,0	0,6667	0,1282	0,01147	0,00603	0,20	0,4790

4.4.2 HS

Table 2: Material properties Hardening Soil model

HARDENING SOIL (HS)	Weight		Strength parameters				Stiffness parameters				others	
Material	γ_{unsat} [kN/m³]	γ_{sat} [kN/m³]	c'_{ref} [kPa]	φ' [°]	ψ [°]	R_{inter} [-]	E_{50}^{ref} [kN/m²]	E_{oed}^{ref} [kN/m²]	E_{ur}^{ref} [kN/m²]	power (m) [-]	ν'_{ur} [-]	K_0 [-]
Dike material Total	18,54	18,54	0	32,8	2,8	0,6667	15000	15000	45000	0,70	0,15	0,4583
Dike material Upper layer	18,54	18,54	3	16,0	0,0	0,6667	15000	15000	45000	0,70	0,15	0,7244
Clay Silty Sandy >17,5 kN/m3	18,73	18,73	0	30,6	0,6	0,6667	15000	15000	45000	0,80	0,15	0,4910
Sand Pleistocene	18,00	20,00	0	31,3	1,3	0,6667	25000	25000	75000	0,55	0,15	0,4805

4.4.3 SHANSEP NGI-ADP

Table 3: Material properties SHANSEP NGI-ADP model

NGI-ADP (SHANSEP)	Weight		Strength parameters		Interface		Stiffness parameters				Interface	others				
Material	γ_{unsat} [kN/m^3]	γ_{sat} [kN/m^3]	alpha (S) [-]	power (m) [-]	c'_{ref} [kPa]	φ' [°]	G/s_u^A [-]	γ_f^C [%]	γ_f^E [%]	γ_f^{DSS} [%]	E_{oed}^{ref} [kN/m^2]	s_u^P/s_u^A [-]	τ_0/s_u^A [-]	s_u^{DSS}/s_u^A [-]	ν [-]	ν_u [-]
Clay Silty 16-17,5 kN/m3	16,82	16,82	0,25	0,80	0,10	22,14	84,34	9,682	13,68	11,68	5333	0,98	0,70	0,99	0,3	0,495

Table 4: Material properties Sheet pile, Anchor, and Base spring

Elastic	Weight	Stiffness parameters		
Material	w $[kN/m/m]$	EA_1 $[kN\ /m]$	EA_2 $[kN\ /m]$	EI $[kN\ m^2\ /m]$
Sheet pile (AZ24-700)	1,368	3,654E6	182,7E3	117,2E3

	Stiffness parameters
Material	EA $[kN]$
Anchor (HTAB 101/20)	974,1E3
Base spring	10E3

4.5 Calculation steps

According to the PPE 6 calculation steps are required to fully analyse the newly designed sheet pile. First, the current dike design should be analysed during daily occurring circumstances. Secondly, the construction should be added, either a sheet pile, an anchored sheet pile, soil-mix blocks etc. and if applicable elevation and widening of the dike. From the moment the construction is added the reduction factor gets added to the sand layer and will stay throughout the following steps. Thirdly the settlement of the soft soils after the installation of the construction should be taken into consideration. This will affect the consolidation state and strength of the soil and therefore, change the forces and moments in later stages. Then finally the dike should be analysed in extreme circumstances, where deformations due to high water levels and maintenance vehicles are considered, and the associated moments and forces. After this, the stability of the dike can be found, together with the safety factor. A summary of all calculation steps is shown in Figure 13. The implementation of these steps within the FEM will be discussed more in Appendix E.

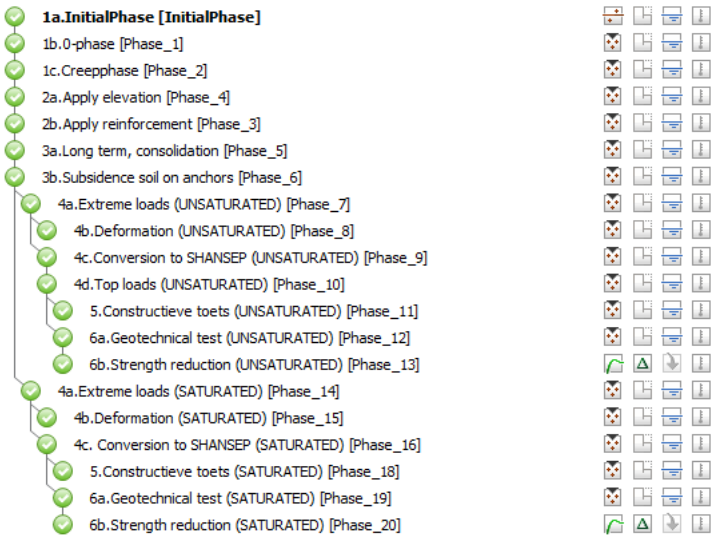

Figure 13: The calculation steps considered in the numerical analysis

5 Virtual experiments performed using the FEM

Using the base model explained in the previous chapters, modifications can be made to analyse the effect of the reduction factor. Two main different altercations from the base model will be made to analyse the effect of the method of implantation of the pre-augering reduction factor. The shape will be modified, but also the value of the reduction factor will be changed. The reduction factor is applied to both the stiffness parameters of the large sand layer and the interface strength factor of the sheet pile.

The current regulation only states a reduction area that reaches in the horizontal direction, while the results of the literature suggest that the influenced area could reach underneath the toe of the sheet pile. By increasing the depth of the reduction area from 0m to 1m, 2m, and 3m, the effect of verticality of the reduction area will be explored. The horizontal area currently spans a distance of 1 meter, to find the effect of the horizontal area on the sheet pile design, widths of 0.5, 1.5, and 2 meters are taken.

As a final modification, different reduction factors are utilized. Instead of a factor of 0.5, values of 0.40, 0.45, 0.55, and 0.60 are taken. This is based on the Wolferen-Sprok research where some soil parts increase in cone resistance while others decrease by 80%. The reduction of 80% is not representative of the entire sand layer, however, it does show the possibility of high reductions. Thus, the maximum factor of 60% is chosen, resulting in a reduction factor of 0.40. The 0.60 factor is chosen based on the largest mean reduction over the sand layer, seen at Wolferen-Sprok, which was 40%. All tests performed are shown in Table 5.

Table 5: Performed tests

Nr.	Value (-)	Depth (m)	Width (m)
1	0,40	0	1
2	0,40	1	1
3	0,40	2	1
4	0,40	3	1
5	0,40	0	0.5
6	0,40	0	1.5
7	0,40	0	2
8	0,45	0	1
9	0,45	1	1
10	0,45	2	1
11	0,45	3	1
12	0,45	0	0.5
13	0,45	0	1.5
14	0,45	0	2
15 (base)	**0,50**	**0**	**1**
16	0,50	1	1
17	0,50	2	1
18	0,50	3	1
19	0,50	0	0.5
20	0,50	0	1.5
21	0,50	0	2
22	0,55	0	1
23	0,55	1	1
24	0,55	2	1
25	0,55	3	1
26	0,55	0	0.5
27	0,55	0	1.5
28	0,55	0	2
29	0,60	0	1
30	0,60	1	1
31	0,60	2	1
32	0,60	3	1
33	0,60	0	0.5
34	0,60	0	1.5
35	0,60	0	2

6 Results & Discussion

To check the validity of the reinforcement, it is crucial to conduct a series of systematic tests set in European standards and PPL. Among these tests, five are specifically dedicated to assessing the integrity of the sheet pile, containing tests to validate whether the stability, the internal strength (based on normal force and moments), the shear strength (based on shear forces), buckling, and sheet pile displacement, remains within the Europeans and PPL standards. Thus, these five tests are employed to analyse the impact of the reduction value on the sheet piles. Further explanation of the formulas and parameters used can be found in Appendix D.

First, all the numerical analyses performed described in Table 5 are analysed using the sheet pile length and design of the base scenario. This entails a sheet pile length of 14,14 m. The stability of the dike changing for the different modifications can be seen in Figure 14 & Figure 15. An obvious general trend can be seen from where the reduction factor influences the stability safety factor. Whenever the reduction factor is higher, the stability is higher. This is only logical, when the stiffness of the soil is reduced less, the soil will experience fewer strains, thus increasing the stability of the sheet pile within the sand layer.

The difference caused by horizontal or vertical modifications is more difficult to observe. Horizontal changes in reduction area size do not show significant changes, most reduction values stay within a delta safety factor of 0.02, except for the reduction factor of 0.45. The 0.45 reduction value, represented as the blue diamond in Figure 14, shows a changing pattern in terms of the stability safety factor. Ranging from 1.11 to 1.17 without a linear trend along the widths, which is peculiar as it does not follow the linear trend of other reduction factors. The most probable cause is the variability of the mesh within the model. However, if this variability is assumed to be a maximum of 0.03 around the real value, a horizontal trend is not possible to be reliably formed.

The different depts show a similar indifference around the size of the reduction area, as the horizontal modifications. All safety factors stay within the 0.02 deviations between different vertical reduction factor area sizes. When considering the variability in the numerical model, no reliable correlation between depth, width and safety factors can be found.

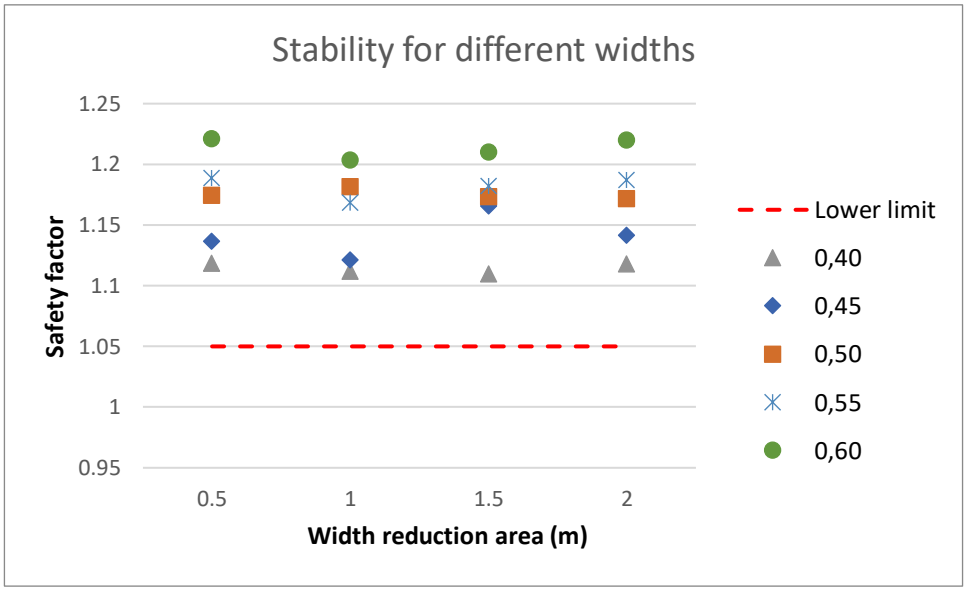

Figure 14: Stability safety factor for changing the reduction factor in the horizontal direction

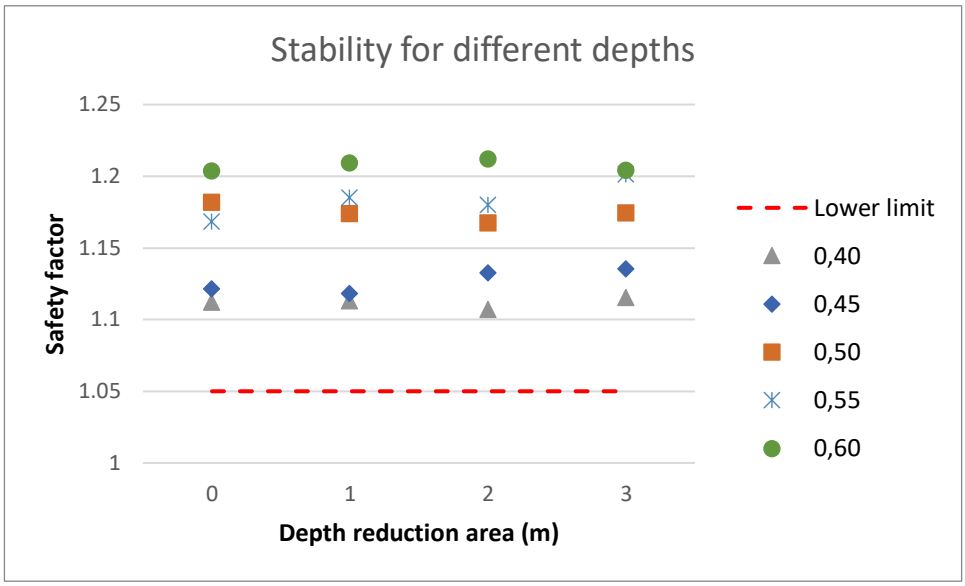

Figure 15: Stability safety factor for changing the reduction factor in the vertical direction

In terms of validation tests for strength and shear strength show very similar results. The numerical analysis reveals minimal deviations when modifying the reduction factor and area. However, the general trend emerges, where a higher reduction value leads to a higher unit check. The unit check is the sheet pile's internal, or shear forces divided by the sheet pile's capacity. A higher unit check indicates a closer proximity to the upper limit. The impact of horizontal and vertical variability, in contrast to the stability, is more apparent in strength and shear strength. Generally, greater depths and widths of the reduction factor result in the sheet pile approaching the limiting value.

Reduction factor widths of 1.0 and 2.0m show the expected distribution based on reduction factors. However, reduction factor widths of 0.5m and 1.5m show surprising results. Especially the reduction values 0.45, 0.55 and 0.60 show great variability within the different reduction areas. For example, the reduction factor 0.60 with 0.5m width portrays an almost equal unit check as the 0.40 reduction factor. Similarly, the 0.55 reduction factor with a 1.5m width shows a similar unit check as the 0.40 reduction factor. Despite the outliers the general trend of the reduction factor combined with the widths displays a positive trend, where both a larger reduction factor and larger width results in a higher unit check. This does not hold for the 0.60 reduction value, where a negative trend is observed. This trend goes against the expected outcome, and it is likely due to variability in the numerical model.

The modifications in depth also show a slightly positive trend between some outliers but to a lesser extent than for the width. This is logical as the forces acting on the sheet pile mostly come from gravity from the soils above, so the soil below the sheet pile will have a smaller impact on the unit check. Trendlines will remain mostly horizontal indicating no effects of depth on the unit check.

Keep in mind, the values obtained through the formulas are significantly influenced by the sheet pile material and the overall dike structure, leading to minor total effects on the unit check. The graphs are shown in Figure 16, Figure 17, Figure 18 & Figure 19.

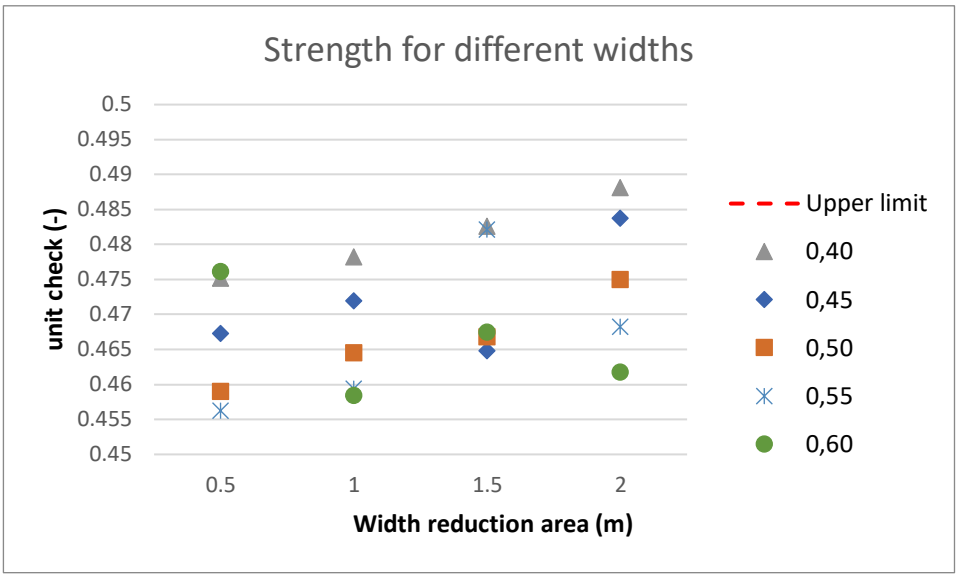

Figure 16: Strength sheet pile for reduction factor area changed in the horizontal direction

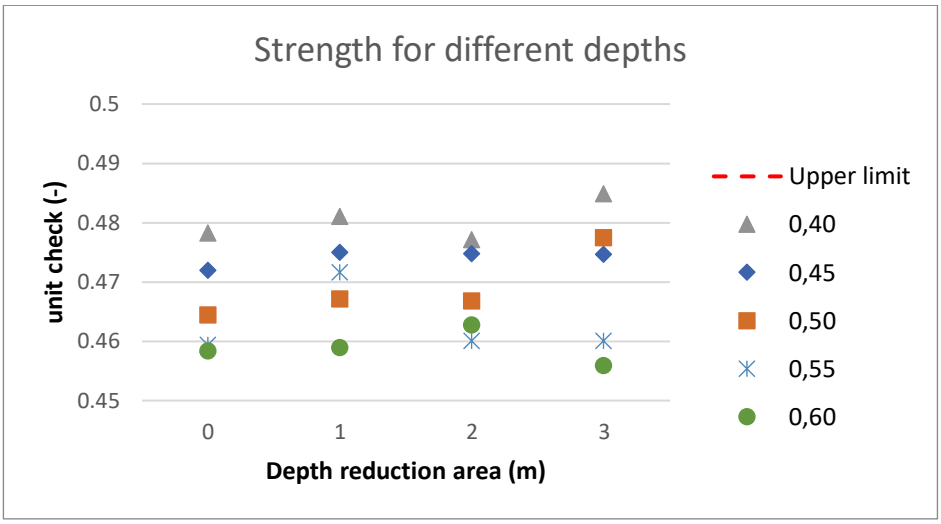

Figure 17: Strength sheet pile for reduction factor area changed in the vertical direction

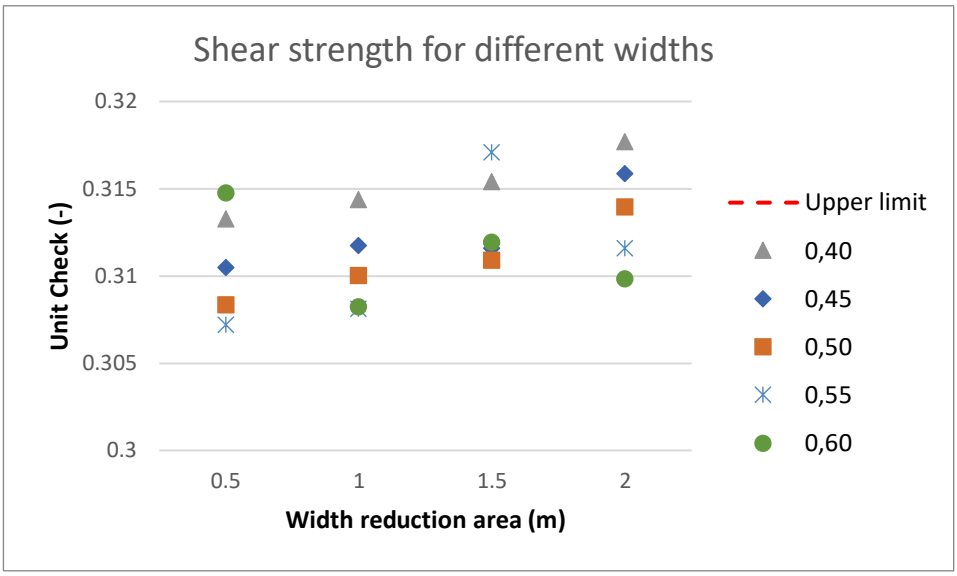

Figure 18: Shear strength for reduction factor area changed in the horizontal direction

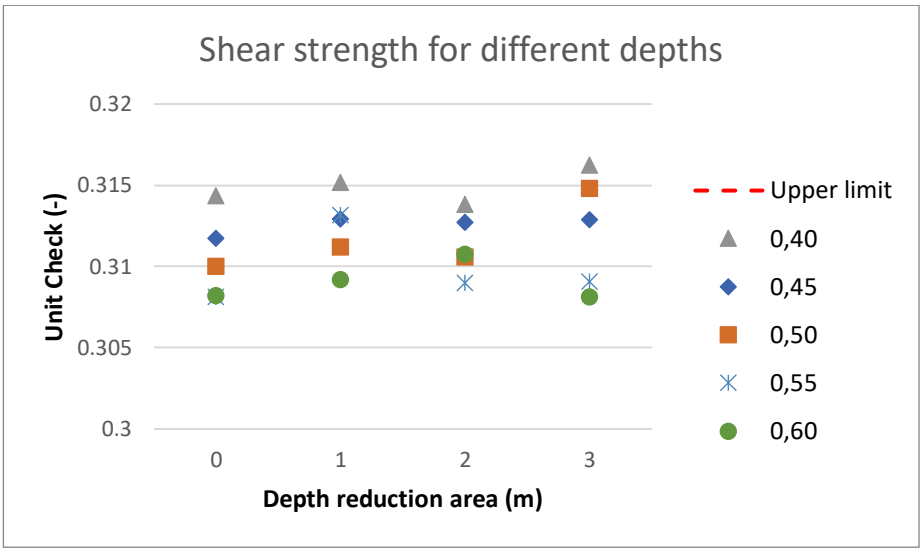

Figure 19: Shear strength for reduction factor area changed in the vertical direction

Regarding the buckling effect validation test, there is a weak relationship between the reduction factor and the amount of buckling observed in Figure 24 & Figure 25. As shown in Appendix F, buckling mainly depends on material properties, and the length of the sheet pile, which remain constant throughout this analysis. Therefore, the only parameter affecting the differences in the sheet pile buckling effect is the normal force. This is seen in the similarities between the strength graphs, however, still some deviations are visible.

The forces acting on the sheet pile are primarily influenced by the entire dike structure, with the reduction zone area playing a minor role. Consequently, most buckling effect points overlap across different reduction factors, with a few exceptions. Again, displaying similar outliers as seen in the strength graphs, the reduction factor 0.60 at 0.5m width, the reduction factor 0.55 at 1.5m width. This shows the dependencies of different validity tests and the susceptibility to outliers.

The width, however, exhibits a similar positive trend as observed in the strength and shear strength validation tests. This is logical as a higher reduction factor reduces the stiffness of the soil surrounding the sheet pile, leading to increased deformations and stresses within the soil. However, the interface

strength has the opposite effect, where a lower value weakens the bond between the soil and the pile. These effects seem to cancel each other out, and only when the area gets larger, primarily increasing the reduced stiffness, does the buckling effect become larger. The depth, however, does not display this positive trendline, again because the area beneath insignificantly influences the forces acting on the sheet pile.

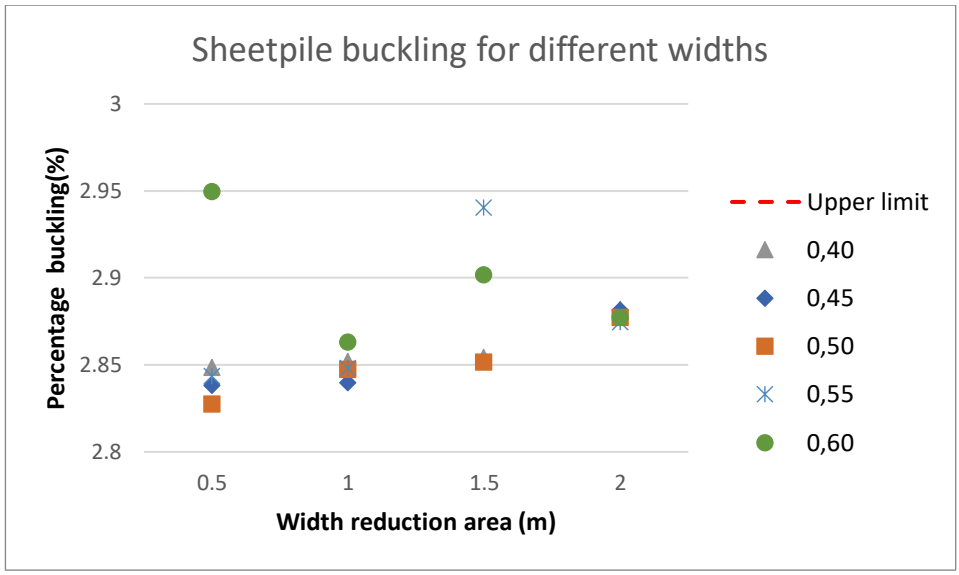

Figure 20: Sheet pile buckling for reduction factor area changed in the vertical direction

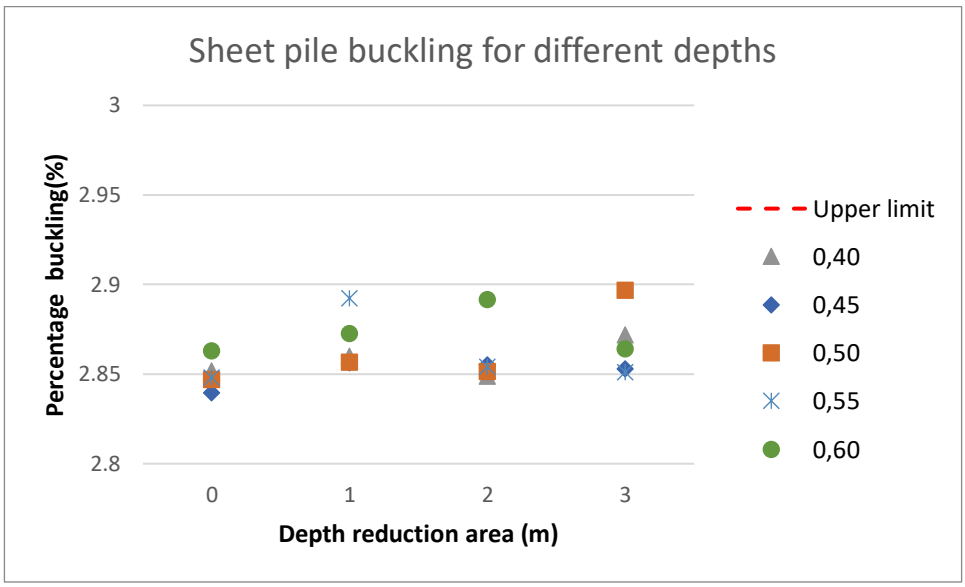

Figure 21: Sheet pile buckling for reduction factor area changed in the vertical direction

The last validation test conducted examines the displacement of the soil, which is the test that exhibits the most significant deviations concerning the reduction factor. The graphs in Figure 22 & Figure 23, depict this. Horizontal displacement is particularly important as it determines the sheet pile validity in this sheet pile design, approaching its maximum allowed limit of 100mm. Displacement also exhibits a clear deviation caused by a reduction factor, with a lower reduction factor resulting in larger displacements. This correlation is sensible as lower stiffness offers less resistance to displacement, while higher stiffness leads to the opposite effect.

Additionally, the width of the reduction factor area also influences the displacement, albeit to a small degree. Greater width corresponds with higher displacement. The reduction factor 0.45 has one outlier showing a deviation from the expected trend, likely again due to variability in the model's mesh, however, the deviations are relatively the largest in comparison with other outliers 10% difference from the expected output in between widths 1 and 2m. This is especially impactful because this is the deciding validity test.

The depth has minimal impact on the displacement, generally maintaining constant values with minor deviation likely attributed to numerical model variability. No exceptional outliers are seen.

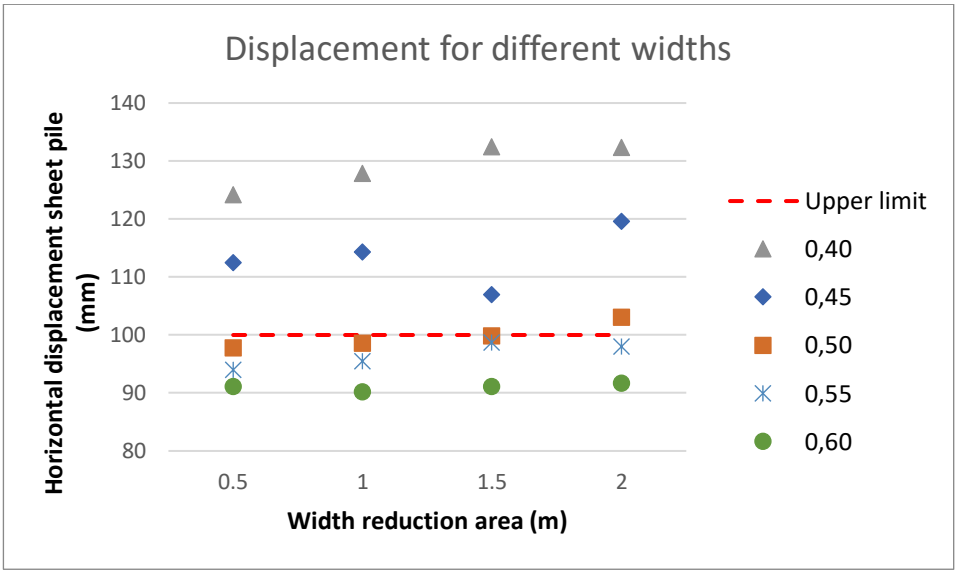

Figure 22: Horizontal displacement sheet pile for changing the reduction factor in the horizontal direction

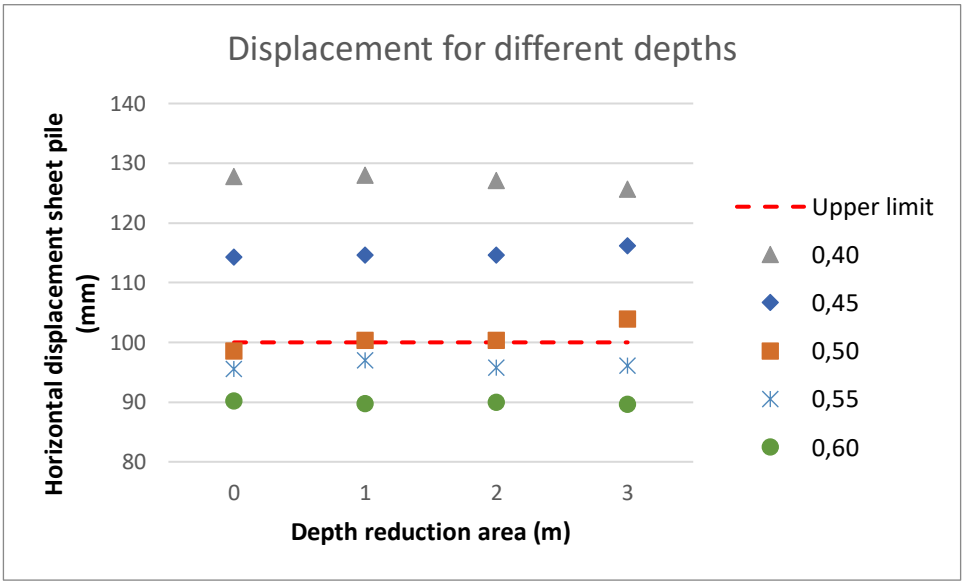

Figure 23: Horizontal displacement sheet pile for changing the reduction factor in the vertical direction

While examining the validation tests along sheet piles of the same length, the largest variation in values arise from modifications of the reduction factor, while only minor trends are observed in the reduction factor area in the variability of the horizontal direction. The depth of the reduction factor area generally exhibits minimal or no noticeable trends, and any trends observed deviate only slightly deviate from the baseline.

The subsequent analysis focuses on determining the valid sheet pile design length for each experiment, the results are shown in Figure 24 & Figure 25. Once again, a clear trend is evident when the reduction factor is altered, with lower reduction factors resulting in longer sheet pile designs and higher reduction factors leading to shorter sheet pile designs. For instance, a reduction factor decreases to 0.4 corresponds to an increase in sheet pile design length of 1.5m. Conversely, the increase of the reduction factor to 0.6 results in a decrease in sheet pile design length of 0.5m.

As the previous analysis on the 14.14m sheet piles, suggested that width had a substantial impact on the sheet pile design, and depth displayed less impactful positive trends, these differences are visible however not as apparent in the sheet pile length. This is mostly due to the fact the sheet pile design length is governed by the displacement where both depth and width only show a small positive trendline.

When the width increases from 1m to 1.5m the sheet pile length increases for a reduction factor of 0.4 but decreases for a reduction factor of 0.45, this can be explained with the outlier seen in Figure 22. The reduction area width of 2m once again shows an increase of sheet pile length again for reduction factors 0.45 and 0.50, by 1m and 0.5m respectively, relative to the original reduction area width sheet pile length. The impact of the depth of the reduction factor area on the sheet pile length is only noticeable when the reduction factor area increases from 0m to 1m depth for reduction factors of 0.45 and 0.50 where a 0.5m increase is observed, any other changes do not induce length changes.

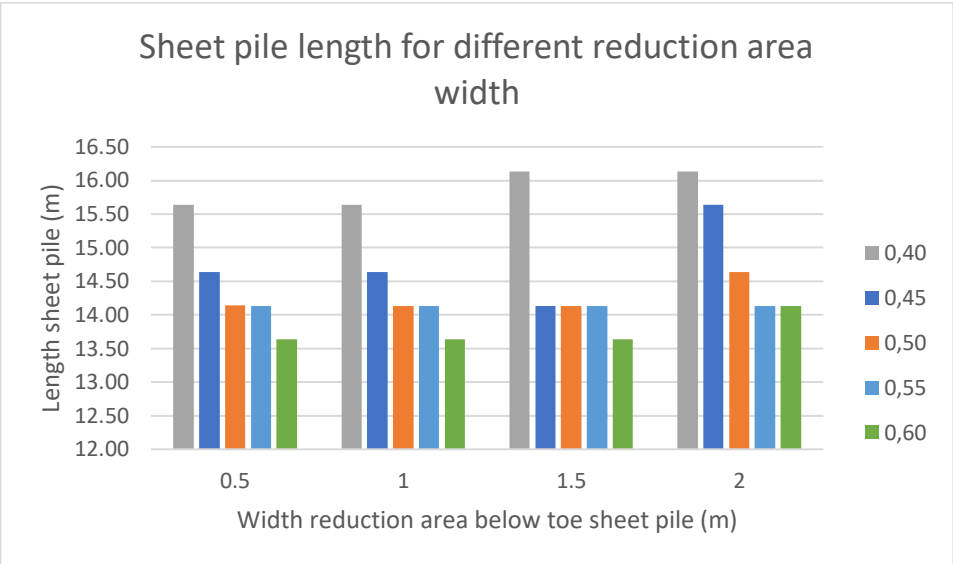

Figure 24: Sheet pile length for changing the reduction area horizontally

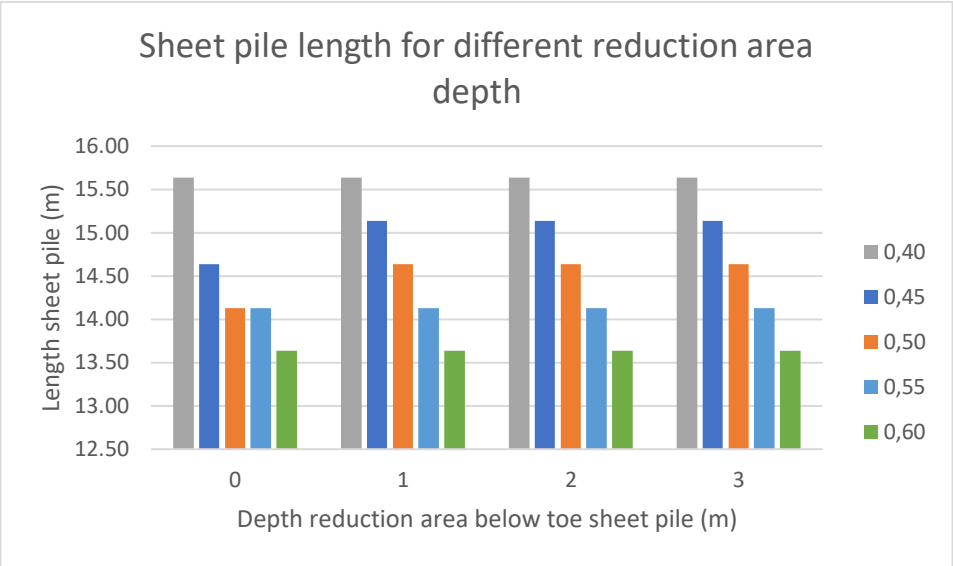

Figure 25: Sheet pile length for changing the reduction area vertically

7 Conclusion

This study aimed to investigate the impact of different implementation methods of the pre-augering installation technique on the design of sheet piles within dikes. Using available data from the literature and recommendation therein, a systematic numerical analysis is performed using the PLAXIS software. Advanced soil models are used, and the reduction factor is applied to simulate the pre-augering installation methods' impact on the soil. Based on this numerical study the following findings were found.

The reduction factor and the area of pre-augering both have an impact on the final sheet pile design. Both factors influence the overall stability and performance of the sheet pile system. However, after detailed analysis, it can be observed that the reduction factor itself has a larger impact on the design compared to the area of pre-augering. From the five sheet pile validity tests, the impact of the reduction factor is significantly the largest on the displacement. The stability factor also shows differences depending on the implementation method, however to a smaller extent. The last three validity tests, concerning the strength, shear strength and buckling of the sheet pile, get influenced to a small extent.

The reduction factor on the interface properties, which represents the reduction in soil stiffness due to the excavation process, directly affects the lateral earth pressure exerted on the sheet pile walls. By considering an appropriate reduction factor, the design can account for the weakened soil conditions and accurately predict the forces acting on the structure. By decreasing the reduction factor from the original 0.5 to 0.4, the sheet pile design increased by 1.5m, which is an increase in sheet pile size of 10%. On the other hand, the decrease of the original reduction factor to 0.6, results in a decrease in sheet pile length of 0.5m.

The area of pre-augering, which refers to the extent of the effect of pre-augering before sheet pile installation, also plays a role in the design. Pre-augering helps create loosened soil for the sheet piles installation process and consequently reduces the lateral earth pressure acting on the walls. However, while it contributes to the overall stability and other sheet pile validation techniques, its impact is relatively less pronounced compared to the reduction factor. Whereas the reduction factor shows differences in sheet pile design ranging from an increase of 1.5m to a decrease of 0.5m, relative to the base scenarios. The enlarging of the depth or width shows a maximum change in sheet pile length of 1.0m.

The sheet pile design is highly influenced by the method of implementation. While the current regulations state a 0.5 reduction factor, the origin of this factor value is inherently wrong, but appropriately assigned based on available information. This analysis shows that if other reduction values are used sheet pile designs will change, either being more cost-efficient or safer.

In conclusion, the reduction factor of pre-augering is an essential consideration in the design of sheet pile systems. The area of the reduction value influences the final design, but only in small amounts. While both factors impact the final design, the reduction factor exerts a larger influence on the stability and performance of the sheet pile system, requiring careful consideration and accurate estimation to ensure a safe and reliable design. The reduction factor itself is currently unknown, while the current pre-augering reduction factor area standards indicate realistic values. It is advised more research is done to find the reduction factor.

The current manner of assessment of the influence of the implementation method of pre-augering comes with some limitations. The biggest limitation of this analysis is the fact that it considers a case study as a foundation for the model. While this ensures a model based on a realistic situation, it is a

specific case which will lack generalizability. The results gained in this study, cannot be reproduced for different situations, and can only be used as qualitative indications. By using a case study, a more complex situation is sketched than a general model would entail, consequently analysing the results takes place in a more complex environment, in which it is more difficult to find correlations.

In addition, as the model is based on the TiWa reinforcement program, the model contains an anchored sheet pile. This reinforces the idea that the model contains complex elements influencing the results, while the study focuses on the sheet pile design, the anchor has not been taken into consideration. Due to time constraints, this has not been investigated. Therefore, the effect the anchor has, or could have had if modified, remains unknown.

The current analysis is based on the design process described by the PPL. By including this framework, a well-defined methodology is used to assess sheet pile design, however, any inaccuracies within this framework, would influence the validity of this study directly. It should be noted that the PPL has been developed and verified by experts, but any oversights, or changes in the future impact this study.

One of the assumptions stated within the PPL is the conversion of the found reduced cone resistance in the literature to soil strength parameters. Currently, the reduction factor influences the stiffness parameter $E_{50}^{ref}, E_{oed}^{ref}$ and E_{ur}^{ref} and interface strength R_{inter}. While other parameters might be influenced as well.

The model's outputs show some large outliers caused by numerical variability. This significantly influenced the possibility to state reliable trends within the validity tests. These outliers could be removed by performing multiple analyses with different meshes. And is advised to do to create a more reliable outcome, however, due to time constraints this was not further pursued in this thesis.

8 References

Arcadis. (2007). *Evaluatie Praktijkproef Fluideren bij Drukken van Damwandplanken.* Arcadis.

Bentley. (2020). *MATERIAL MODELS MANUAL.* Bentley.

Bingxiang Yuan, R. C. (2015). Effect of Sand Relative Density on Response of a Laterally Loaded Pile and Sand Deformation. *Journal of Chemistry*, Volume 2015, Article ID 891212, 6 pages.

Corrie Walton-Macaulay, L. S. (2018). Compacted Unsaturated Soil Behavior in a Large Scale Laboratory Test. *PanAm Unsaturated Soils 2017* (pp. 425-436). Dallas: ASCE.

Daizo Kunii, O. L. (1991). *Fluidization Engineering.* Boston, London, Singapore, Sydney, Toronto, Wellington: Butterworth-Heinemann.

Deltares. (2023, 07 13). *D-Sheet Piling*. Retrieved from deltares: https://www.deltares.nl/software-en-data/producten/d-sheet-piling

(2008). *Eurocode 3: Design of steel structures - Part 5: Piling.* NEN connect.

Grimstad G, A. L. (2011). NGI-ADP: Anisotropic shear strength model for clay. *International Journal for Numerical and Analytical Methods in Geomechanics, Volume 36, Issue 4*, 483-497.

Kames, J. H.-J. (2021). *Praktijkproef onderzoek effecten van Fluideren op conusweerstand Vianen Hazelaarplein.* Tiel: Waterschap Rivierenland.

Lanting Wu, J. S. (2021). Parametric Sensitivity Study of Deep Excavation in Singaport Old Alluvium Formation. *Advances in Civil Engineering, Volume 2*.

Larisch, M. (2014). *Behaviour of stiff, fine-grained soil during the installation of screw auger displacement piles.* The University Of Queensland.

Larissa de Brum Passini, F. S. (2018). Mechanism of model pile installation by water jet fluidization in sand. *Ocean Engineering*, 160-170.

Linger, D. A. (1963). Effect of Vibration on Soil Properties. *Highway Research Record*.

M.D. Larisch, D. W. (2012). *Load Capacity of Auger Displacement Piles.* Brisbane: The University of Queensland.

(2016). *NEN-EN 1997-1+C1 National Annex to NEN-EN 1997-1 Eurocode 7: Geotechnical design –Part 1: General rules.* NEN connect.

Panagoulias S, V. G. (2018). *The SHANSEP NGI-ADP model 2018.* Delft: PLAXIS bv.

Passini L B, S. F. (2015). Installation and Axial Load Capacity of Fluidized Model Piles in Sandy Soils. *Doctoral dissertation, Master's dissertation, Federal University of Rio Grande do Sul]. Federal University of Rio Grande do Sul's repository*, 292.

Rijkswaterstaat. (2015). *Afronding onderzoek vermindering corrosietoeslag damwanden.* Rijkswaterstaat.

Rijkswaterstaat. (2021). *Schematiseringshandleiding macrostabiliteit.* Rijkswaterstaat.

S. Thorburn, D. G. (1993). The response of sands to the construction of continuous flight auger piles. *Proceedings of the 2nd international geotechnical seminar on deep foundation on bored and auger piles*, 429-443.

Schanz T, V. P. (1999). The hardening-soil model: Formulation and verification. *Beyond 2000 in Computational Geotechnics*, 281-290.

Sweco. (2021). Dijkversterking Tiel - Waardenburg toelichting. Gelderland: Gemeente West Betuwe.

Tsinker, G. (1988). Pile Jetting. *Journal of Geotechnical Engineering*, 326-334.

Van der Meer, M. N. (2004). *Technisch Rapport Waterspanning bij dijken Waterkeringen (TAW).* Rijkswaterstaat, DWW.

Vermeer P A, N. H. (1999). A soft soil model that accounts for creep. *Beyond 2000 in Computational geotechnics*, 249-261.

Waterschap Rivierenland. (2020). *Rapport Vergunningen Ontwerp (VO) TiWa.* Waterschap Rivierenland.

Zawnenburg, C. V. (2013). *Technisch rapport macrostabiliteit.* Deltares.

9 Appendix

A. Literature research

Nederlek/Vianen-Hazelaarplein comparison

Table 6: Comparison of characteristics of the two fluidization studies

Kenmerk (Characteristic)	HHSK H6 Opperduit	WSRL Hazelaarplein
Damwandplank (Sheet pile)	AZ26 (dubbel (geponste profielen))	AZ24-700 enkel
Lengte (length)	20,0 m	15.,5m
Lengte damwand in zand (length in sand)	Ca. 7m	Ca 7m
Lengte damwand in deklaag (length in cover)	Ca. 13m	Ca 8m
Nozzle aantal (amount of nozzles)	2 (per dubbele plank) (per double sheet pile)	1 per plank (per sheet pile)
Locatie nozzel (Location nozzles)	0,6m onder puntniveau damwand (0,6m underneath foot sheet pile)	Puntniveau damwand (At the foot of the sheet pile)
Orientatie nozzel (Orientation nozzle)	Richting rivierzijde (Towards riverside)	Richting rivierzijde (Towards riverside)
Druk Machine (Pressing Machine)	Super crush Piler SCZ 675 WM	Woltman THW5525
Maximale drukkracht (Maximal press-in force)	120 ton	160 ton
Trilmachine	Onbekend	Dosan
Trilblok (Vibratory Hammers)	Dieseko HF 2332 VM	Dieseko 23VMA
Aantal sonderingen voor (Number of probes before)	2	9
Aantal sonderingen na (Number of probes after)	2	9
Sondering voor datum (Date of probes before)	16-05-2007	22-01-2021
Realisatie damwand (Instalment of sheet pile)	06-06-2007	05-02-2021
Sondering na datum (Date of probes after)	14-06-2007	05-03-2021
Verschil dagen voor – na (difference in days before – after)	8	28
Gemiddelde druk zandpakket (Mean pressure sandlayer)	40 bar	44 bar
Gemiddeld debiet zandpakket (Mean discharge sandlayer)	150l/min	70l/min
Gemiddelde Qc zand t.h.v inklemming damwand (Mean Qc sand at the sheet pile retainment)	Ca. 19 Mpa	Ca. 7Mpa
Gemiddelde Qc zand t.h.v inklmeming damwand (Mean Qc sand at the sheet pile retainment)	Ca. 10Mpa	Ca. 6Mpa

Wolferen-Sprok analysis

Table 7: Mean cone resistance and change for location 3 throughout the depth

Soil type (3a)	Topsoil layer [m NAP] (3a)	Bottom soil layer [m NAP] (3a)	Mean cone resistance [MPa]		Percentual change [%]
			3a	3b	
Sand	10,0	8,6	1,5	1,6	+7
Veen	8,6	8,0	1,3	1,4	+8
Clay, silty	8,0	6,8	3,0	0,9	-71
Peat	6,8	6,3	0,6	0,6	-5
Sand	6,3	4,3	7,5	1,4	-81
Clay, silty	4,3	2,8	1,7	1,5	-13
Sand, slightly consolidated	2,8	0,6	13,0	3,3	-74
Sand, slightly consolidated	0,6	-0,4	10,9	14,2	+30
Sand, highly consolidated	-0,4	-2,0	28,7	20,1	-30
Sand, slightly consolidated	-2,0	-4,6	28,0	20,0	-28

Table 8:Mean cone resistance and change for location 4 throughout the depth

Soil type (4a)	Topsoil layer [m NAP] (4a)	Bottom soil layer [m NAP] (4a)	Mean cone resistance [MPa]		Percentual change [%]
			4a	4b	
Sand	10,0	8,6	2,2	1,5	-32
Clay, silty	8,6	7,1	1,1	0,7	-39
Peat	7,1	6,0	1,3	0,5	-60
Sand	6,0	4,2	6,0	5,4	-10
Clay, silty	4,2	2,5	2,0	2,3	+14
Sand, slightly consolidated	2,5	-0,4	12,1	17,6	+46
Sand, highly consolidated	-0,4	-2,6	24,9	18,2	-27
Sand, slightly consolidated	-2,6	-4,6	19,9	17,8	-11

B. Soil models

Soft Soil Creep

The Soft Soil Creep (SSC) model has incorporated the creep behaviour seen in soft soil such as clay and peaty soils. Features of this model consist of stress-dependent stiffness; differences in primary loading and unloading or reloading, the creep behaviour, so the time-depended compression, and the memory of pre-consolidation stress. The model uses the Mohr-Coulomb failure criterion, which uses a linear representation of the critical shear stress defined by:

$$\tau_f = \sigma \tan(\phi) + c$$

Equation 1

With τ_f being the shear stress at failure, c is the soil's cohesion, ϕ the soil's friction angle, and σ is the principal stress.

The SSC model also uses the Modified Cam-Clay to describe the creep yield surface as an ellipse. And with the associated flow rule, meaning a yield function acts as a plastic potential. Which describes the direction and magnitude of the plastic deformation, concerning the stress state of the material undergoing plastic deformation. The flow rule states that the plastic strain vector points perpendicular to the yield function.

The main assumption in the SSC model is that it uses an additive composition of strain. The strain gets divided into the $\dot{\varepsilon^e}$, the elastic strain, and the $\dot{\varepsilon^c}$, the creep strain. Non-failure situations will not take ε^c into account instantaneously but will behave elastically until a certain stress threshold has been exceeded. The idea from Bjerrum (1967) that pre-consolidation stress is entirely dependent on the previously accumulated creep strain is also adopted in this model.

$$\dot{\varepsilon} = \dot{\varepsilon^e} + \dot{\varepsilon^c}$$

Equation 2

Elastic behaviour

Hooke's law has been used in the SSC model to model the linear elastic behaviour of soft soils. This states that the strain is directly proportional to the stress until the elastic limit is reached. The *Modified Cam Clay Model* uses a similar manner to model elastic behaviour using both the elasticity modulus and Poisson's ratio to determine unloading-reloading behaviour. The elasticity modulus E_{ur} can be characterized using the bulk modulus K_{ur}, and Poisson's ratio v_{ur}.

$$E_{ur} = 3K_{ur}(1 - 2v_{ur}), \qquad K_{ur} = \frac{p' + c\cot(\phi)}{\kappa^*}.$$

Equation 3

The bulk modulus is stress-dependent according to the $K_{ur} = \frac{p' + c\cot(\phi)}{\kappa^*}$ rule. From these rules, the elastic volumetric behaviour of the soft soil is found.

$$\dot{\varepsilon}_v^e = \frac{\dot{p'}}{K_{ur}} = \kappa^* \frac{\dot{p'} + c\cot(\phi)}{p'}$$

Equation 4

Where κ^* is the modified swelling index, and p' is the effective mean stress acting on the node. So, the elastic strain in the SSC model is controlled by the mean stress p'.

Creep behaviour

The volumetric strain in the creep strain phase is calculated using the equation below.

$$\dot{\varepsilon}_v^c = \frac{\mu^*}{\tau}\left(\frac{p^{eq}}{p_p^{eq}}\right)^{\frac{\lambda^*-\kappa^*}{\mu^*}}$$

Equation 5

Where λ^* and κ^* are the modified compression and swelling indexes, μ^* is the modified creep index, p^{eq} is the stress based on the current stress state of the numerical step, p_p^{eq} is the pre-consolidated stress, and τ is one day, incorporating the time-dependent component.

The figure below shows a visual representation of the formula, where anywhere within the red and dotted blue line elastic behaviour is exerted, and the creep is negligibly small. When the yield surface is reached, the soil reaches the state of creep, where plastic deformation will take place. However, as the strain increases the yield function together with the plastic potential will change as well, which can be seen in Equation 7.

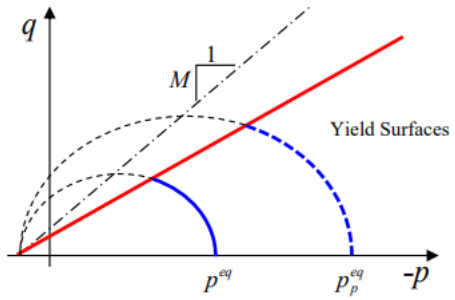

Figure 26: Yield surfaces of the SSC model, Mohr Coloumb yield surface (red) and elliptical caps for the calculations of viscoplastic strains (blue)

It should be noted that τ has been chosen based on the assumption that all inelastic strains are time-dependent.

After an external load is applied, the stress on each node in three-dimensional spaces is found within the FEM model, and then the equivalent pressure (p^{eq}), combining the three dimensions in a single value, can be calculated using the following equation.

$$p_{eq} = p' + \frac{q^2}{M^2\,(p' + c\cot(\phi))}$$

Equation 6

Where p' is the mean effective stress on the node, q is the deviatoric stress and M is the soil parameter representing the critical state line $M = \frac{6\sin(\phi)}{3-\sin(\phi)}$.

To incorporate the history of consolidation on in the model the pre-consolidated stress is used within the model. This parameter is based on the initial pre-consolidated stress p_{p0}^{eq} and the volumetric strains in the history of the soil.

$$p_p^{eq} = p_{p0}^{eq} \exp\left(\frac{\varepsilon_v^c}{\lambda^* - \kappa^*}\right)$$

Equation 7

The modified soil parameters are found using existing soil parameters. The modified soil parameters can be converted to conventional soil parameters, using formulas formulated in the Material Model Manual (Bentley, 2020)

As of now, the creep strain has been defined with a volumetric strain, however, soft soils exhibit deviatoric strains during the creep phase. To model general creep strains the flow rule has been adopted since it is assumed that creep strain a time-dependent plastic strain is. Using the normal flow rule the following equation is found.

$$\dot{\varepsilon^c} = \lambda \frac{\delta g^c}{\delta \underline{\sigma'}}$$

Equation 8

Where the plastic potential function is described as the equivalent pressure:

$$g^c = p^{eq}$$

Equation 9

From the above equation, the following equation can be found.

$$\dot{\varepsilon_v^c} = \dot{\varepsilon_1^c} + \dot{\varepsilon_2^c} + \dot{\varepsilon_3^c} = \lambda \left(\frac{\delta p^{eq}}{\delta \underline{\sigma_1}'} + \frac{\delta p^{eq}}{\delta \underline{\sigma_2}'} + \frac{\delta p^{eq}}{\delta \underline{\sigma_3}'}\right) = \lambda \frac{\delta p^{eq}}{\delta_p'}$$

Equation 10

Hardening Soil

The hardening soil model is a constitutive double-stiffness model described by Schanz and Vermeer in 1999. It is used to simulate the behaviour of soils under primary loading conditions and captures the stress-strain response to loading in a non-linear fashion using progressive stiffening of soils under loading conditions. Two stress-dependent stiffnesses are incorporated within this model, like the Cam-Clay model and the Duncan-Chang model, both the initial loading and the unloading-reloading are used to find the total strains. This model attempts to reduce the inconsistencies found in other double-stiffness models, caused by using a hypo-elastic model, firstly by using an elasto-plastic type of model. Doing so the model will capture the difference between loading and unloading more consistently. Secondly by introducing soil dilatancy, and thirdly by introducing a yield cap.

In the hardening soil model, the soil is represented by a multi-surface yield criterion that defines the limit of the soil's strength. When the stress state exceeds the yield surface the elastic behaviour of the soil shifts to plastic behaviour. The key feature of this model is the isotropic hardening of the soil, the material's strength increases uniformly in all directions as plastic deformation increases, both deviatoric and hydrostatic strain. The hardening of soil is separated into two types: shear and compression hardening. Shear hardening covers the hardening caused by deviatoric loading, whereas compression hardening covers the hardening caused by primary compression loading. The frictional hardening is modelled with the non-associated flow rule, whereas for the cap hardening an associated flow rule is assumed.

The yield surface can be visualized in the picture below. Where the blue line indicates the cap, which shows the elasticity boundary for the p-axis. And the red line indicates the yield surface caused by the deviatoric stresses. Both surfaces can grow due to the soil's stiffness that grows along with an increase in stresses.

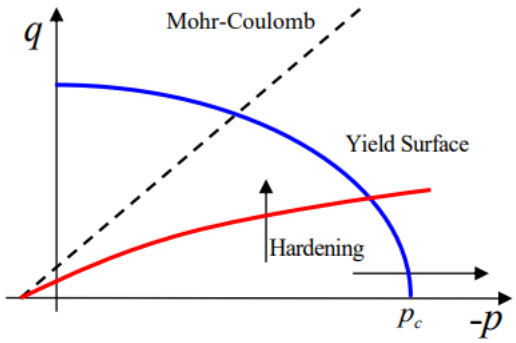

Figure 27: The yield surfaces of the HS model

Deviatoric Hardening Mechanism

Like the Duncan-Chang model, the HS model is designed to incorporate the hyperbolic relationship between the vertical strain ε, and the deviatoric stress q, comely observed in primary triaxial loading. This yield surface due to deviatoric stresses can be represented as a hyperbolic curve, defined with the equation.

$$\varepsilon_q^{p-shear} = \frac{1}{E_i}\frac{q}{1-q/q_a} - \frac{q}{E_{ur}} \text{ for: } q < q_f$$

Equation 11

Where q is the deviatoric stress, E_i is the initial elasticity modulus, E_{ur} is the elasticity modulus in unloading-reloading phases, and $\varepsilon_q^{p-shear}$ is the deviatoric plastic strain caused by only the deviatoric stresses.

The Mohr-Coulomb yield surface has also been incorporated within this model, using the ultimate friction angle (ϕ) and the cohesion (c) to characterize soil strength, and the ultimate deviatoric stress q_f can be calculated.

$$q_a = \frac{q_f}{R_f}, \qquad q_f = \frac{2\sin(\phi)}{1-\sin(\phi)}(c\cot(\phi) - \sigma_3')$$

Equation 12

As soon as the deviatoric stress reaches the failure criterion q_f plastic deformation will occur. The asymptotic deviatoric stress q_a can be calculated using the failure ratio R_f (with a default value of 0,9)

One of the stress-dependent stiffness moduli is the stiffness modulus for unloading-reloading E_{ur}.

$$E_{ur} = E_{ur}^{ref}\left(\frac{c\cos(\phi) + \sigma_1\sin(\phi)}{c\cot(\phi) + p^{ref}\sin(\phi)}\right)^m$$

Equation 13

Where E_{ur}^{ref} is the reference elasticity modulus for unloading and reloading at the reference pressure p^{ref}, which is taken as a default value advised by PLAXIS at 100 kN/m^2. By doing so the unloading and reloading path is purely elastic. The power m indicates the stress dependency of the elastic modulus and ranges from 0,5 to 1,0. Where 1,0 indicates a soft soil, and 0,5 a hard soil.

The yield surface is defined using one other parameter, the initial elastic modulus E_i.

$$E_i = \frac{2E_{50}}{2-R_f}, \qquad E_{50} = E_{50}^{ref}\left(\frac{c\cos(\phi)+\sigma_3'\sin(\phi)}{c\cos(\phi)+p^{ref}\sin(\phi)}\right)^m$$

Where E_{50} is the confining stress-dependent stiffness modulus for primary loading, which is based on the reference stiffness modulus, E_{50}^{ref}, corresponding to the reference stress p^{ref}. It shows a similar equation as the unloading reloading stiffness modulus.

The image below illustrates the hyperbolic curve simulated by the HS model.

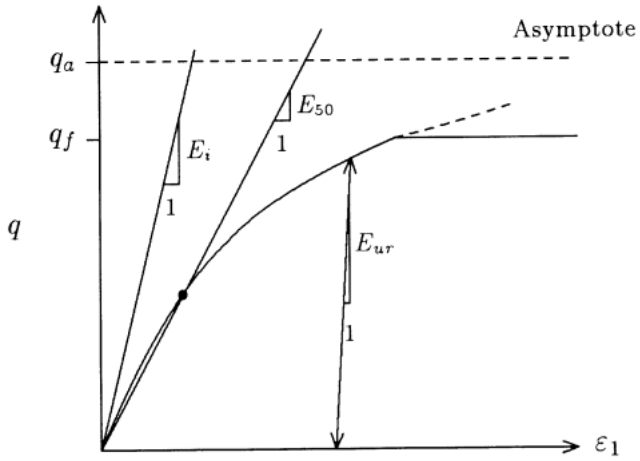

Figure 28: Hyperbolic stress-strain curve in a drained compression triaxial test

The flow rule in this model is defined such that the plastic deviatoric strain and the volumetric strain are related in the following manner.

$$\varepsilon_v^{p-\dot{s}hear} = \sin(\psi_m)\, \varepsilon_q^{p-\dot{s}hear}$$

Equation 14

Where $\varepsilon_v^{p-shear}$ is the plastic volumetric strain, $\varepsilon_q^{p-shear}$ is the plastic deviatoric strain, and ψ_m is the mobilized dilation angle.

To find the mobilized dilation angle Rowe's theory (1962) is used. Using both the mobilized friction angle, ϕ_m, and the critical state friction angle, ϕ_{cv}. The critical state friction angle comes with the idea that materials will compress if the mobilized friction angle is larger than the critical state friction angle and will dilate if reversed.

$$\sin(\psi_m) = \frac{\sin(\phi_m) - \sin(\phi_{cv})}{1 - \sin(\phi_m)\sin(\phi_{cv})}$$

Equation 15

$$\sin(\phi_m) = \frac{\sigma_1 - \sigma_3}{\sigma_1 + \sigma_3 - 2\cot(\phi)}$$

Equation 16

$$\sin(\phi_{cv}) = \frac{\sin(\phi) - \sin(\psi)}{1 - \sin(\phi)\sin(\psi)}$$

Equation 17

Where ψ is the ultimate dilation angle.

Volumetric Hardening Mechanism

The volumetric hardening mechanism can be visualized with the cap, the yield surface enclosing the elastic domain on the x-axis. The cap is an elliptical shape defined by the following equation.

$$F_c = \left(\frac{q^*}{\alpha}\right)^2 + p^2 + p_c^2 = 0$$

Equation 18

Where p_c is the intersection of the volumetric yield surface with the p-axis, and α is the shape factor of the ellipse. The q^* is the stress invariant and is defined as:

$$q^* = \frac{q}{f(\theta)}, \qquad f(\theta) = \left(\frac{3-\sin(\phi)}{2\left(\sqrt{3}\cos(\theta)-\sin(\theta)\sin(\phi)\right)}\right)$$

Equation 19

The volumetric plastic strain calculated using the cap is considered for p_c.

$$\varepsilon_v^{p-cap} = \frac{\beta}{1-m}\left(\frac{p_c}{p_{ref}}\right)^{1-m}$$

Equation 20

Where ε_v^{p-cap} is the plastic volumetric strain caused by the cap, β is another parameter influencing the shape of the ellipse, p_{ref} is again the reference stress parameter and m is the strength characteristic of the soil.

α and β are not used as inputs for the models but are derived from the combination of other parameters. In specific the parameters K_0^{nc} and E_{oed} are used. Whereas the E_{50}^{ref} mostly controls the deviatoric yield surface, the E_{oed}^{ref} mostly controls the volumetric yield surface. Both k_0^{nc} and E_{oed} can be found by using formulas based on oedometer tests, which are given by PLAXIS.

SHANSEP NGI-ADP

The SHANSEP NGI-ADP model is intended for anisotropic undrained soil strength conditions. And makes sure dikes can be analysed according to the new standards for designing dikes applied in the Netherlands within a FEM environment. This model is a slight adaptation to the original NGI-ADP model (Grimstad, Andresen & Jostad (2010)). The modification includes the ability to use the effective stress state of the soil to simulate the potential changes of the undrained shear strength S_u.

SHANSEP

SHANSEP is an abbreviation for Stress History and Normalized Soil Engineering Properties and is a model to simulate undrained shear strength of soft soils. The following equation is used to describe the undrained shear strength given a certain stress path.

$$S_u = \alpha\sigma_1' \left(\frac{\sigma_{1,max}'}{\sigma_1'}\right)^m = \alpha\sigma_1'(OCR)^m$$

Equation 21

Where α and m are normalised soil parameters.

The usual method in SHANSEP is to calculate the undrained shear strength and OCR using the vertical effective stress σ_v', however, in the SHANSEP NGI-ADP model, the design choice was made to use the effective major principal stress σ_1'. The thought process behind this choice is that this is the major principal stress that will give the highest compressive value, independent of the axial directions. When the vertical effective stress would be considered for soils within a slope the OCR and S_u would present lower values than σ_1'.

NGI-ADP model

The NGI-ADP model is a model that may be used to analyse the undrained loading of clay, in terms of deformation, capacity and soil structure. Which makes it compatible with dikes under extreme conditions, where undrained conditions are applicable. The essentials of the NGI-ADP model can be described in four points:

- Three different stress paths/states input parameters for (undrained) shear strength are used: Active, Direct Simple Shear, and Passive. (ADP)
- The yield surface is based on a translated approximated Tresca criterion
- Plastic failure strains and shear strengths in arbitrary stress paths are modelled using elliptical interpolation functions
- Isotropic elasticity, given by the unloading/reloading shear modulus, G_{ur}

The modified Tresca yield criteria featured in the NGI-ADP model account for the difference in undrained shear strength in both compression and extension.

$$f = \left|\tau - (1-\kappa)\tau_0 - \kappa\frac{s_u^C - s_u^E}{2}\right| - \kappa\frac{s_u^C + s_u^E}{2} = 0, \quad \kappa = 2\frac{\sqrt{\gamma^p/\gamma_f^p}}{1+\gamma^p/\gamma_f^p} \text{ when } \gamma^p < \gamma_f^p \text{ else } \kappa = 1$$

Equation 22

Where $\tau = 0.5(\sigma_v' - \sigma_h')$, s_u^C is the undrained shear strength in compression, s_u^E is the undrained shear strength in expansion, κ is a stress path-dependent hardening parameter to account for difference in failure shear strain in compression and extension, using both γ^p and γ_f^p being the plastic shear strain and the failure plastic shear strain, respectively.

This yield criterion can be transformed so it can be used in a 2 dimensions plane strain.

$$f = \sqrt{\left(\frac{\sigma_{yy} - \sigma_{xx}}{2}(1-\kappa)\tau_0 - \kappa\frac{s_u^A - s_u^P}{2}\right)^2 + \left(\tau_{xy}\frac{s_u^A - s_u^P}{2s_u^{DSS}}\right)^2} - \kappa\frac{s_u^A + s_u^P}{2} = 0$$

Equation 23

This incorporates the active, direct shear sample, and passive shear strength (ADP) s_u^A, s_u^{DDS}, s_u^P.

The yield criteria in the plane strain can be plotted as an elliptical-shaped curve in a plane strain deviatoric stress plot. Seen in Figure 29.

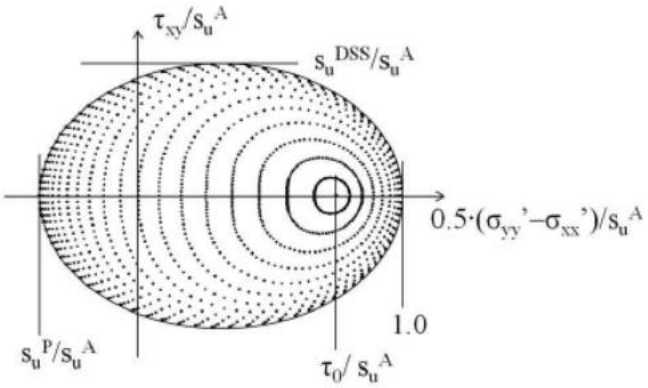

Figure 29: Typical deviatoric plane strain plot of equal shear strain contours for the NGI-ADP model (Bentley, 2020)

For further information about the implementation of the NGI-ADP model, the PLAXIS material model manual can be used.

Combination

The main difference between the original NGI-ADP model and the SHANSEP NGI-ADP model is the calculation of the undrained shear strength, where SHANSEP uses Equation 21, and NGI-ADP normally uses Equation 24. The variation in depth considered is valid in the case of horizontal soil layers, where the reference depth stays fixed. However, due to the incline present in dikes, this is not realistic. It would mean that the undrained shear strength would increase along the surface of the slope because the depth changes. By using the SHANSEP method of obtaining S_u this problem is omitted.

$$s_u^A(y) = s_{u,ref}^A + (y_{ref} - y)s_{u,inc}^A \text{ for } y < y_{ref}$$

Equation 24

The SHANSEP NGI-ADP model shows the advantage over the original NGI-ADP model, by giving a realistic, empirical way of modelling the undrained shear strength.

C. Structure model

Sheet pile

The elastic behaviour for sheet piles is modelled by using the in-plane axial stiffness EA_1, the out-of-plane axial stiffness EA_2, the elastic bending stiffness EI, and Poisson's ratio v. PLAXIS uses the Mindlin beam theory as described by Bathe (1982). This means that in addition to normal bending shear deformation is considered. The shear stiffness of the sheet pile is found by using:

$$Shear\ stiffness = \frac{5EA}{12(1+v)}$$

Equation 25

For anisotropic plates, the following stress-strain relationship is used:

$$\begin{bmatrix}\sigma_N \\ \sigma_2 \\ \tau\end{bmatrix} = \begin{bmatrix}E_1 & 0 & 0 \\ 0 & E_2 & 0 \\ 0 & 0 & kG\end{bmatrix}\begin{bmatrix}\varepsilon_N \\ \varepsilon_2 \\ \gamma\end{bmatrix}$$

Equation 26

Where $E_1 = \frac{EA_1}{d}$,$E_2 = \frac{EA_2}{d}$, $G = \frac{E_1}{2}$, and $k = \frac{5}{6}$.

Anchor & base spring

The anchor's elastic behaviour uses the relationship between axial force N and the elongation u described by the following equation:

$$N = \frac{EA}{L}u$$

Equation 27

Where EA is the anchor stiffness and L is the length. The bending is not considered.

The base spring is only used as a material fixing the sheet pile in the vertical direction, representing the toe resistance, which is otherwise not considered.

For the complete model, the material model manual from PLAXIS can be reviewed (Bentley, 2020).

D. Geometry model

Figure 30: Study area Tiel-Waardenburg dike reinforcement project (Sweco, 2021)

E. Calculation steps

Current situation

The first step of analysing a new dike reinforcement design is to analyse the current situation and initialize the model's stresses acting within the soil. This is done while assuming drained conditions within the soil, as the only force acting on the dike is gravity acting on the dike body. Without any heavy loads acting on the during the current daily situation, drained conditions are justifiable.

The actual implementation within Plaxis is split up into three steps:

1a. The initial phase

This is the phase PLAXIS 2D uses to calculate the stresses acting within the dike. The k0 procedure is a built-in calculation method that considers the loading history of the soil. When this calculation method is called PLAXIS 2D generates vertical stresses that are in equilibrium with the self-weight of the soil. Note that PLAXIS 2D does not generate shear stresses so a complete stress field equilibrium is not ensured. However, due to the relatively horizontal surface, the k0 method can still be used followed by a plastic nil-phase, where small equilibrium corrections take place.

1b. Plastic nil-phase

In the plastic nil-phase, no additional loads are added on the dike, but small corrections to find complete stress field equilibrium will be made. After this phase, all stresses will obey the failure condition.

1c. Creep phase

When the dike is at the end of its lifespan, the geometry of the dike should be subjected to a creep phase where the settlement of the soil during the lifespan of the dike is taken into consideration. To simulate this a period of 10 years is included where the creep of, predominantly, the soft soils is calculated.

All three phases use the model shown in Figure 12.

Installation of structure

After the stresses and settlement within the current design are calculated, the proposed construction designs can be entered. In the case of TiWa DWP190 both a reconstruction of the dike body and an additional anchored sheet pile are added, so two steps are considered.

2a. Apply elevation

2b. Apply reinforcement

These steps still use drained soil conditions, as no large loads are added. In these stages, the geometry is changed according to the new design (see Figure 31), and the anchored sheet pile is added (see Figure 32). From this phase onward the effect of pre-drilling is also entered into the model seen as the purple area within the sand. All following phases should contain the 0.5 reduction in soil strength. PLAXIS 2D will again find the new stresses acting on the new dike. When inserting the sheet pile into the model a base spring is added to keep the sheet pile vertically in place during the settlement phases. This is done to reduce the underestimation of the stresses acting on the anchor during phase 3.

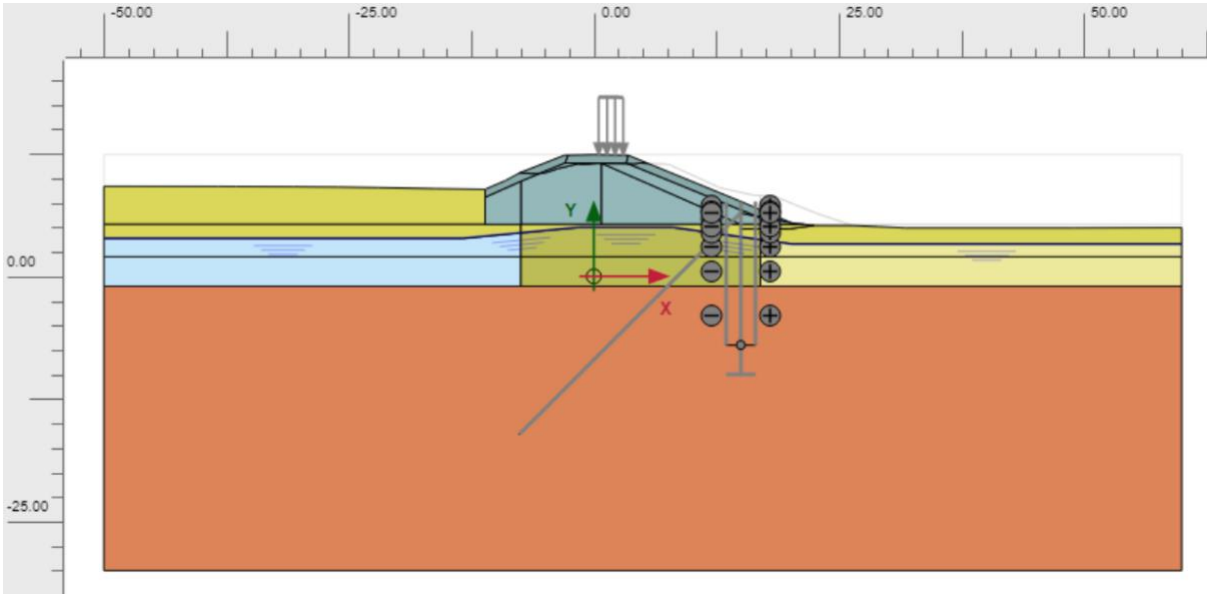

Figure 31: The model after applying elevation

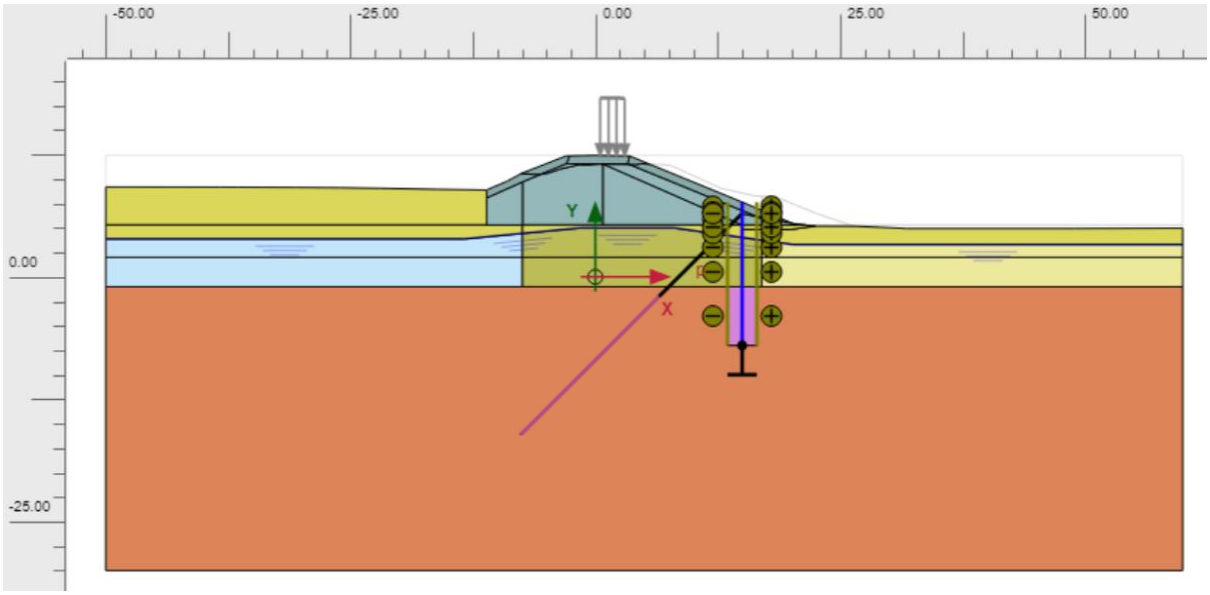

Figure 32: The model after applying the reinforcement construction

Long-term settlement on structure

3a. Long term, settlement

During the next step consolidation during the lifetime of the soil is calculated. However, it should be noted that this step is not to see the effect of consolidation on the geometry, but instead for the stresses acting on the soil body and the longitudinal reinforcement. The settlement of the soil causes negative skin friction on the sheet pile, essentially pulling the sheet pile down. This in combination with a high point resistance at the toe of the sheet pile, will increase the buckling effect and vertical stability in the sheet pile, and potentially reach a failure. These increases in normal force due to the settlement cannot be overlooked, however, the actual buckling test will be done in phase 5.

3b. Settling ground on construction

The creep effect is calculated using a time-dependent creep calculation for a 100-year time period using the SSC model. During phase 3a. the settlement of 100 years is calculated, from where afterwards, during phase 3b. the effect on the construction, in specific the anchor, is simulated. As the anchor will be under high pressures of consolidating soil.

Extreme situation analysis

Then finally the analysis of extreme situations will take place. From this step forward two different situations will be considered, and both follow the same procedure. One situation with only high water levels using a normal schematised phreatic flow, the other one with high water levels and overtopping causing a completely saturated dike, meaning the phreatic flow will follow the contours of the dike. Four separate steps are taken in phase 4 to accommodate the changes in the model and to assess the dike.

4a. Extreme hydraulic loads

The model will assume high hydraulic loads with drained conditions and calculate the stresses throughout the dike. The hydraulic loads, meaning, the phreatic plane, the groundwater level, and the capillary rise, are all considered when defining the model. This is done according to the Technical Report Water stresses (Van der Meer, 2004) the Technical Report Marcrostability (Zawnenburg, 2013) and the Schematization manual Macrostabiliteit (Rijkswaterstaat, 2021). As mentioned before the two different versions tested will use different types of hydraulic loads depending on the saturation assumption. Another change in the model is the removal of soil behind the sheet pile, simulating the extreme situation where water has washed away the soil. The models from this phase can be seen in Figure 33 & Figure 34. (The different colours in the top layer only indicate different levels of mesh coarseness, not different soil parameters)

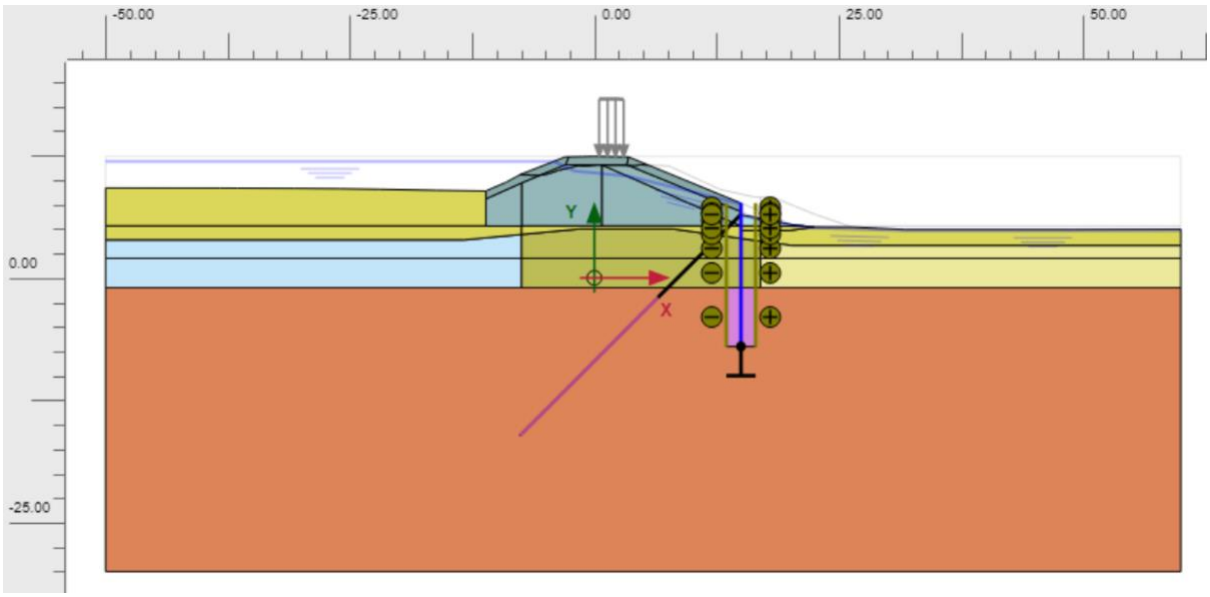

Figure 33: The model in extreme circumstances (unsaturated)

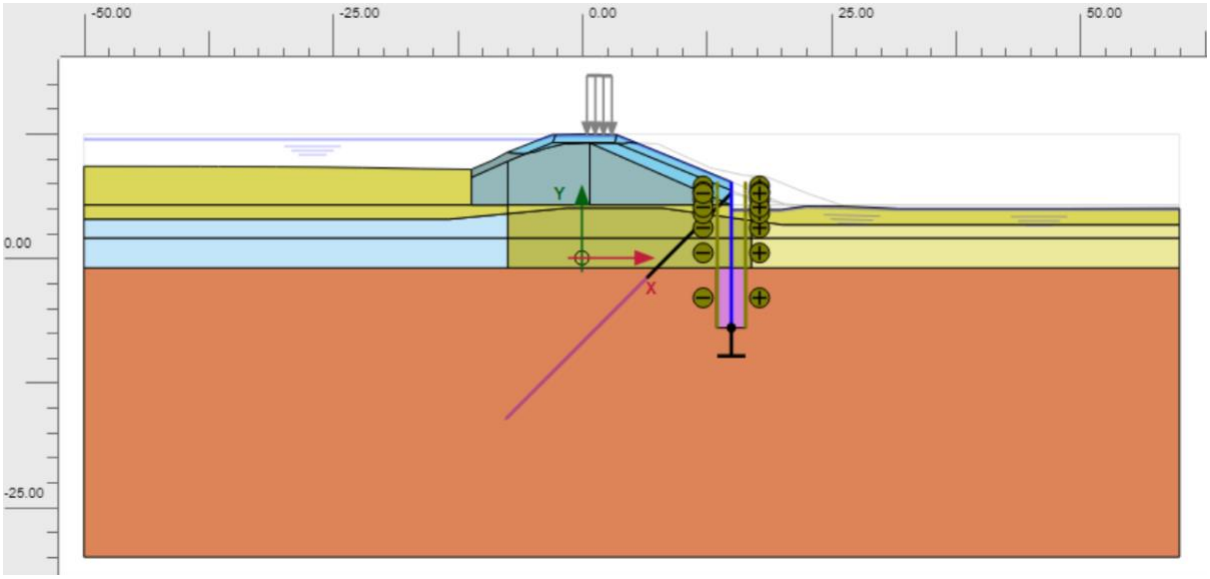

Figure 34: The model in extreme circumstances (saturated)

4b. Deformation

When the stresses during the extreme hydraulic loads have been calculated, then the base spring keeping the sheet pile in place during other phases can be removed to calculate the actual deformation in the dike due to the extreme conditions. When the base spring is removed, all individual components can freely move horizontally and vertically. Additionally in the unsaturated case, the vehicle load is added to simulate the most extreme conditions.

4c. Conversion to SHANSEP

During undrained conditions caused by the extreme vehicle loads during maintenance in high water level events, and during the slip surface calculations the soil models will change to the Shansep NGI-ADP model. The combination of the Shansep and the NGI-ADP model uses the initial stresses while including the stress history to find the undrained shear stress. And considers the undrained shear stress in different parts of the slip surface; the active, neutral, and passive parts. A more detailed description can be found in section 4.4.3. Only the clay layers will be converted, the sand or sandy layers will remain in the Hardening soil model (Section 4.4.2)

4d. Vehicle top loads

When the conversion is made the deformations and stresses caused by the maintenance vehicle loads can be considered in the model as a preparation for the construction and stability tests. This is only done during unsaturated circumstances, because during saturated circumstances it can be assumed that no vehicle can safely access the area, due to wave overtopping and the slippery saturated clay layers, and therefore no large top loads can exist.

Construction test

5. Construction test

During the constructive test, the forces and moments on the reinforcement will be calculated during high water events and if applicable with top loads due to vehicles. The construction test is used to test whether the structure can withstand the large moments and forces acting on the dike. The sheet pile is again fixed by using a base spring at the toe of the dike, by doing this the forces stay within the sheet pile instead of being translated to movement. Using this assumption underestimation of the forces

acting on the sheet pile will not occur. In this, and the following phases an added design approach is added where the friction angle, cohesion and undrained shear strength are multiplied by a factor to add a factor of safety.

Dike stability

6a. Geotechnical test

Finally, the macro stability of the dike is considered when the base spring is again released and the overall stability of the dike during extreme conditions is checked.

6b. Strength reduction

Then when the dike remains stable the safety factor is calculated by using the strength reduction method. This method reduces, like the name suggests, the strength stepwise until failure occurs. The strength reduction method gives similar safety factors as obtained from the Limit Equilibrium Method (LEM) slip-circle analysis.

F. Result calculations

First of all, it is essential to ensure the stability of the dike under extreme conditions outlined in phase 6b. It is during this phase that the safety factor for stability can be determined and outputted. The safety factor should remain above the safety standard $\gamma_{b;GEO}$.

$$\sum M_{SF} \geq \gamma_{b,GEO}$$

Equation 28

Secondly, the strength of the sheet pile should be high enough. If the sheet pile cannot withstand the large forces and moments acting on it, it will cut through the sand creating failure possibilities. The stress exerted at the toe of the sheet pile, $\sigma_{s;dw;d}$, cannot exceed the yield stress of the steel sheet pile, $f_{y;dw;d}$.

$$\sigma_{s;dw;d} = \frac{M_{s;d}}{W_{open}} + \frac{N_{s;d}}{A_{corr}} \leq f_{y;dw;d}$$

Equation 29

Where $M_{s;d}$ and $N_{s;d}$ represent the maximum moment and the maximum force exerted on the sheet pile, respectively, while accounting for some extra safety factors defined below, W_{open} denoting the pile's moment of resistance of its cross-section after corrosion, and A_{corr} is the area of the pile's cross-section after corrosion.

$$N_{s;d} = f_{open} * \gamma_{add;N} * \gamma_{b;str} * N_{s;\max M;EEM}$$

Equation 30

$$M_{s;d} = f_{open} * \gamma_{add;m} * \gamma_{b;str} * M_{s;max;EEM}$$

Equation 31

Where f_{open} represents the openness factor of the sheet pile, $y_{add,N}$ and $\gamma_{add;m}$ corresponds to the load effect factor on normal force and moments, respectively. $\gamma_{b,str}$ denotes the schematization factor, and $N_{s;max;EEM}$ representing the maximum normal force found in phase 5 within the simulation.

Thirdly, the sheet pile should be able to withstand the shear forces, $Q_{s;d}$, according to the material norms. Eurocode 3 part 5 gives the following formula to check the ability to withstand shear forces.

$$Q_{s;dw;d} \leq Q_{r;d}$$

Equation 32

Where

$$Q_{s;dw;d} = \frac{A_{v;corr} * f_{y;dw;d}}{\sqrt{3}}$$

$$Q_{r;d} = f_{open} * \gamma_{b:str*}\gamma_{add;Q} * Q_{s;max;EEM}$$

And where $A_{v;corr}$ is the shear area body after corrosion and $Q_{s;max;EEM}$ is the maximum shear force in the sheet pile found in phase 5.

Furthermore, the occurrence of buckling, resulting from the combination of significant normal forces, substantial moments, and the presence of a lengthy sheet pile, can serve as a critical failure

mechanism. The following formula is used according to NEN EN1993-5 to find the critical buckling load.

$$N_{cr} = EI\beta_D\pi^2/l^2$$

Equation 33

Where E represents the elasticity modulus of the sheet pile, I denotes the moment of inertia of the cross-sectional area of the pile, β_D is the reduction value, and l is the effective length of the sheet pile. This should be checked against $N_{s;d}$ described previously.

$$\frac{N_{s;d}}{N_{cr}} \leq 0{,}04$$

Equation 34

Lastly, the displacement of the sheet pile should be considered. The maximum horizontal displacement according to phase 4, $u_{x;max;dw}$, together with the partial factor that accounts for uncertainties in calculation methods, γ_d, cannot exceed the norm set by the PPL.

$$u_{x;max;dw} * \gamma_d \leq u_{x;d;dw}$$

Equation 35

Most parameters used in these validity tests are either material properties or calculation factors including uncertainties caused by schematization or by the model.

Table 9: values for parameters for the calculations

Parameters	Source
$\gamma_{b,GEO} = 1{,}05$	Spreadsheet (1)
$f_{open} = 1{,}00$	Value given for a continuous sheet pile
$\gamma_{add;N} = \gamma_{add;m} = \gamma_{add;Q} = 1{,}00$	(NEN-EN 1997-1+C1 National Annex to NEN-EN 1997-1 Eurocode 7: Geotechnical design –Part 1: General rules, 2016)
$\gamma_{b;str} = 1{,}10$	Spreadsheet (1)
$\beta_D = 1{,}00$	(Eurocode 3: Design of steel structures - Part 5: Piling, 2008)
$f_{y;dw;d} = 355\ N/mm^2$	Eurocode 3
$W_{open} = 1648\ cm^3/m$	Sheet pile AZ24-700 (Rijkswaterstaat, 2015)
$A_{corr} = 114{,}4\ cm^2/m$	Sheet pile AZ24-700 (Rijkswaterstaat, 2015)
$A_{v;corr} = 30{,}5\ cm^2/m$	Sheet pile AZ24-700 (Rijkswaterstaat, 2015)
$I_{corr} = 37616\ mm^4$	Sheet pile AZ24-700 (Rijkswaterstaat, 2015)
$E = 210\ GPa$	General elasticity modulus steel

1	This value, is project specific and can be found using a spreadsheet, developed and validated by POVM, integrating the WBI relation damage and flood risk

G. Result plots